Electronic Supplementary Material (ESI) for Chemical Communications

Supporting Information

Making practical use of the *pseudo*-element concept: an efficient way to ternary intermetalloid clusters by an isoelectronic Pb^-/Bi combination

Rodica Ababei,[a] Johanna Heine,[a] Małgorzata Hołyńska,[a] Günther Thiele,[a] Bastian Weinert,[a] Xiulan Xie,[a] Florian Weigend,[b] and Stefanie Dehnen*[a]

[a] Fachbereich Chemie, Wissenschaftliches Zentrum für Materialwissenschaften, Philipps-Universität Marburg, Hans-Meerwein-Straße, D-35043 Marburg, Germany, email: dehnen@chemie.uni-marburg.de; [b] Karlsruher Institut für Technologie (KIT), Institut für Nanotechnologie, Hermann-von-Helmholtz-Platz 1, 76344 Eggenstein-Leopoldshafen, Germany

Contents:

1. Synthesis details

General: All manipulations and reactions were performed under dry argon or nitrogen atmosphere and the absence of light using standard Schlenk or glovebox techniques. Metallic films are obtained under daylight owing to photochemical decomposition; therefore, upon several unsuccessful attempts to gain the desired products, the Schlenk tubes have been generally wrapped in aluminum foil, which served to receive crystalline products in good yields. All solvents were dried and freshly distilled prior to use. [2.2.2]crypt[1a] (Cryptofix, Merck) was dried in vacuum for 13 h. Ni(cod)2 was synthesized according to the literature[1b] and $ZnPh_2$ (Acros Organics, 95%) was dried in vacuum for 13 h.

Syntheses of K(Pb,Bi)$_2$: $K(Pb,Bi)_2$ was prepared by fusion of stoichiometric amounts of the elements at 970°C for 2 days in a sealed niobium tube, enclosed in a fused silica jacket that was in turn evacuated and flame-sealed. Upon this procedure, the sample was water-quenched. The resulting compound is dark gray and brittle, but shiny with metallic luster. The product was pulverized inside a glove-box.

Syntheses of [K([2.2.2]crypt)]$_2$[Pb$_2$Bi$_2$]·en (1): The as-prepared $K(Pb,Bi)_2$ phase (500 mg, 1.098 mmol) and [2.2.2]crypt (500 mg, 1.328 mmol) were transferred into a Schlenk tube. At room temperature 25 mL of ethane-1,2-diamine (*en*) were added. The mixture was allowed to stir for 1 h, and the readily obtained reddish brown mixture was left to stand for 12 hours. The solution was decanted from the alloy residue, and large dark reddish brown plate crystals of **1** (710 mg, 0.412 mmol, 75% based on Pb) were grown by slow evaporation under reduced pressure. Energy-dispersive X-ray (EDX) spectroscopy analyses of several crystals confirmed the composition of **1** (see below).

Syntheses of [K([2.2.2]crypt)]$_2$[Pb$_7$Bi$_2$]·1.36en (2): Compound **2** was prepared in a similar reaction as compound **1**, followed by a different crystallization technique. After filtration through a standard glass frit, the resulting solution was layered by toluene. After 48 h, black plate crystals of **2** formed at the wall of the Schlenk tube in lower yield (150 mg, 0.054 mmol, 34% based on Pb) as in the case of **1**. EDX analyses of several crystals confirmed the composition of **2** (see below).

Syntheses of [K([2.2.2]crypt)]$_3$[Ni$_2$Pb$_7$Bi$_5$]·2en·2tol (**3**): 204 mg (0.125 mmol) of $[K(2.2.2\text{-crypt})]_2[Pb_2Bi_2]$·*en* were dissolved in *en* (3 mL), resulting in a dark reddish-brown solution. 44 mg (0.163 mmol) of $Ni(cod)_2$ were suspended in *en* (1 mL), whereupon a yellow suspension was obtained. The suspension was added to the solution while stirring vigorously. The reaction mixture was allowed to stir for 3 hours. It was then filtered through a standard glass frit, and the resulting, reddish brown solution was carefully layered with toluene (*tol*, 4

mL). After 2 days, dark brown plates of **3** crystallized at the wall of the Schlenk tube in approximately 95 mg yield (0.023 mmol, 64% based on Pb). EDX analyses of several crystals confirmed the composition of **3** (see below).

Syntheses of [K([2.2.2]crypt)]$_4$[Zn@Zn$_5$Pb$_3$Bi$_3$@Bi$_5$] (4): 204 mg (0.125 mmol) of [K(2.2.2-crypt)]$_2$[Pb$_2$Bi$_2$]·*en* were dissolved in *en* (3 mL), resulting in a dark reddish-brown solution. 33 mg (0.l50 mmol) ZnPh$_2$ were suspended in *en* (1 mL), whereupon a colorless suspension was obtained. The suspension was added to the solution while stirring vigorously. The reaction mixture was allowed to stir for 3 hours. It was then filtered through a standard glass frit, and the resulting, reddish brown solution was carefully layered with toluene (*tol*, 4 mL). After 2 days, black plate-like crystals of **4** crystallized at the wall of the Schlenk tube in approximately 75 mg yield (0.017 mmol, 55% based on Bi). EDX analyses of several crystals confirmed the composition of **4** (see below).

2. ^{207}Pb NMR spectroscopy

Methods: Single crystals of **1** were dissolved in *en* or DMF under inert gas and the NMR tube was sealed. ^{207}Pb NMR spectra in *en* were recorded at 25°C on a Bruker Avance 500 spectrometer, operating at 104.6 MHz. The spectrometer is equipped with a 5 mm BBO probe with z-gradient. ^{207}Pb NMR studies in DMF were performed at variable temperatures on a Bruker 400 spectrometer operating at 83.67 MHz. A Bruker standard single pulse sequence was used. In order to define the resonance signal, several spectra with a spectral width of 800 ppm were first recorded to cover the whole chemical shift range (−6000 to +6000 ppm). The final spectrum was acquired with a spectral width of 400 ppm, a typical relaxation delay of 0.3 s, and 160 000 to 240 000 scans. A typical experiment time was about 20 hours. The chemical shift of ^{207}Pb was referenced to Me$_4$Pb (δ = 0.0 ppm) and the spectra were processed with Bruker Topspin 3.0.

Results: One broad peak was observed at −3861 ppm (K(Pb,Bi)$_2$) or −3875 ppm (**1**, Figure S1), with line widths of $\Delta\nu_{1/2}$ = 2100 Hz or 2135 Hz at 25 °C. The observed signals are almost ten times as broad as those of two other known lead clusters $[NiPb_{10}]^{2-}$ ($\Delta\nu_{1/2}$ = 280 Hz) and $[PtPb_{12}]^{2-}$ ($\Delta\nu_{1/2}$ = 198 Hz) at similar temperature.[2] We dedicate the observed slight difference of the chemical shift (14 ppm) and the signal width (35 Hz) as deriving from a slightly different ratio of the various species that form the dynamic equilibrium in solution, since much larger differences in the chemical shifts are expected if the solutions contain different species (c.f. a chemical shift of 1167 or −996 ppm for $[Ni@Pb_{12}]^{2-}$ or $[Ni@Pb_{10}]^{2-}$, respectively).[2]

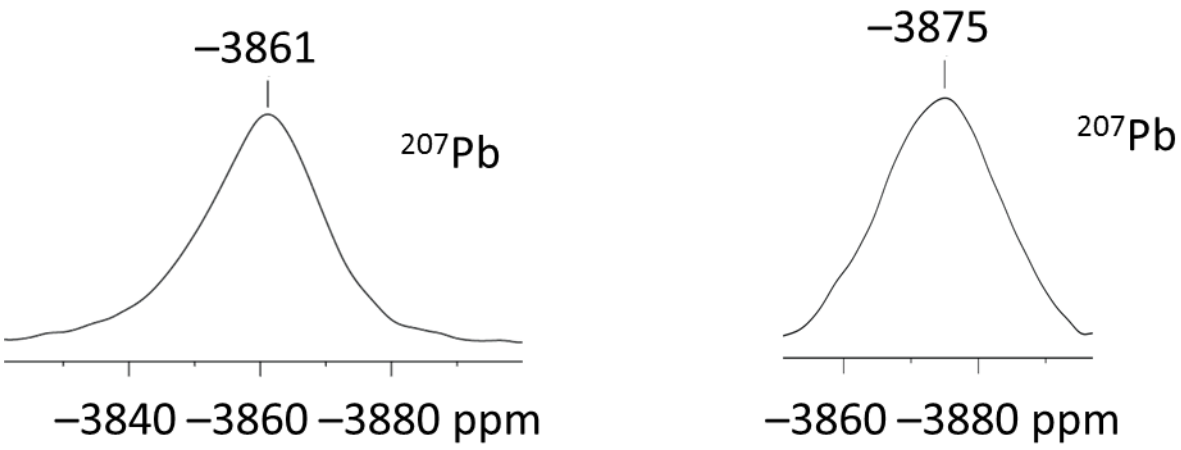

Figure S1. ^{207}Pb NMR signal of a solution of the K(Pb,Bi)$_2$ alloy (left) and single crystals of **1** in *en* (right).

Measurements in DMF at 25, 5, and −15°C result in line widths of 3800, 3000, and 1800 Hz. A slight difference in the ^{207}Pb chemical shift was also observed between the two solvents, which is subject to a currently undertaken, more comprehensive investigation on solvent effects at binary Pb/Bi anions.

Attempts to record NMR spectra at elevated temperature (60 °C) in *en* caused the sample to decompose. Attempts to receive NMR data of compounds **3** and **4** have not been successful – possibly due a variety of different species/fragments in solution in combination with different types of Pb atoms.

3. Single crystal X-ray crystallography

Data of the X-ray diffraction analyses: T = 100(2) K, MoK$_\alpha$-radiation ($\lambda_{Mo\text{-}K\alpha}$= 0.71073 Å), graphite monochromator, imaging plate detector system STOE IPDS2T. Structure solution by direct methods, full-matrix-least-squares refinement against F^2; software used SHELXL-97.[3a] Table S1 summarizes data collection and refinement details. Graphics were generated by using Diamond 3 software.[3b]

Table S1. X-ray data collection, structure solution and refinement data of **1** - **4**.

Compound	**1**	**2**	**3**	**4**
Empirical formula	$C_{38}H_{80}O_{12}N_6K_2Pb_2Bi_2$	$C_{38.63}H_{74.72}Bi_2K_2N_{6.63}O_{12}Pb_7$	$C_{72}H_{124}Bi_5K_3N_{10}Ni_2O_{18}Pb_7$	$C_{72}H_{144}Bi_8O_{24}K_4N_8Zn_6Pb_3$
Formula weight /g·mol^{-1}	1723.62	2770.64	4147.76	4347.98
Crystal color, shape	reddish brown, plate	black, plate	dark brown, plate	black, plate
Crystal size /mm^3	0.12 × 0.05 × 0.04	0.03 ×0.10 × 0.16	0.09 × 0.16 × 0.19	0.25 × 0.14 × 0.01
Crystal system	monoclinic	hexagonal	monoclinic	triclinic
Space group	$P2_1$	$P6_3/m$	$C2/c$	$P\bar{1}$
a /Å b /Å c /Å	12.158(3) 20.619(4) 12.581(3)	12.212(3) 26.414(4)	29.707(5) 13.204(3) 28.242(4)	18.463(4) 28.665(5) 28.935(5)
α /° β /° γ /°	 118.92(3) 	 	 107.24(3) 	62.70(3) 88.33(3) 71.68(3)
V /Å^3	2761(2)	3411(2)	10580(3)	12798(4)
Z	2	2	4	4
ρ_{calc} /g·cm^{-3}	2.074	2.697	2.604	2.257
μ(MoK$_\alpha$) /mm^{-1}	12.64	22.51	19.90	16.17
2θ range /°	3.82-58.52	3.08-49.98	3.02-50.00	3.02-58.46
Reflections measured	16860	21763	39809	106680
Independent reflns, R(int)	12203, 0.1494	2018, 0.1708	9268, 0.1580	63556, 0.1981
Independent reflns ($I > 2\sigma(I)$)	6596	1347	5642	11163
Parameters	559	128	431	1789
Restraints	73	4	13	825
R_1 ($I > 2\sigma(I)$)	0.0841	0.0571	0.0730	0.0884
wR_2 (all data)	0.1893	0.1520	0.1298	0.1739
GooF (all data)	1.004	1.023	1.043	0.867
Flack[3c]	0.02(2)	–	–	–
Max. peak / hole /e$^-$·Å^{-3}	2.09 / −3.82	1.21 / −1.55	1.69 / −1.73	2.94 /-2.10
Absorption correction type[3d]	numerical	numerical	numerical	gaussian
Min. / max. transmission	0.337 / 0.702	0.054 / 0.454	0.070 /0.768	0.164/0.618

3.2 Details of the structure refinements:

Where possible, H atoms were placed in calculated positions and treated with a riding model.

Compound $C_{38}H_{80}O_{12}N_6K_2Pb_2Bi_2$ (1): The structure of **1** was solved in the non-centrosymmetric space group $P2_1$. As for the isomorphous compound comprising the homologue anion $[Sn_2Bi_2]^{2-}$, attempts to switch it into a centrosymmetric space group result in chemically unreasonable models. For the cluster anion, occupational disorder was assumed with each atom site occupied by Pb/Bi (constrained half-occupancies and EXYZ/EADP constraints used). ISOR restraints were applied to selected light atoms (O4, C4, C29, C25, C9, C8, C35, O7, C32, C3, C26, C13). On the final difference Fourier map, the highest maximum of 2.09 e/Å^3 is located at 1.35 Å from Bi4. Figure S2 shows the packing of cations and anions in the crystal structure of compound **1**.

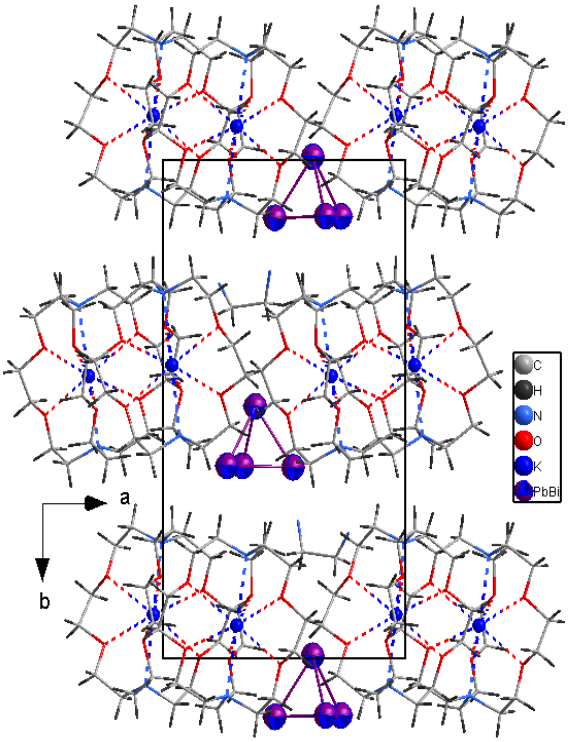

Figure S2. Packing of anions and cations in the crystal structure of compound **1**, viewed along the crystallographic *c*-axis. Selected distances within the anion (see Figure 1 in the main manuscript) [pm]: Pb/Bi−Pb/Bi 3.013(2)-3.048(2) Å.

Compound $C_{38.63}H_{74.72}Bi_2K_2N_{6.63}O_{12}Pb_7$ ***(2):*** The structure of **2** was solved in the non-centrosymmetric space group $P6_3$ and subsequently switched to $P6_3/m$. A careful check for the possibility of merohedral twinning was carried out. In the resulting structure model, two symmetry-independent heavy metal atom (Pb/Bi) positions were found. One position is general, the latter is of *m* (Wyckoff symbol *6h*) site symmetry. Taking into account the results of further analyses (Pb:Bi = 7:2) and the space group symmetry operations, the only possible assignment is Pb for the general position and Pb/Bi with 0.167 and 0.333 occupancies for the special position. The Pb atom on the general position had to be split into two half-occupancy components during further refinement cycles. The complex $[K([2.2.2]crypt)]^+$ cation lies on a special position (three-fold axis). The remaining content includes heavily disordered ethylenediamine molecules occupying two sites. In both cases, the molecules are disordered with respect to a three-fold axis, lying on special or general positions. For one molecule, the occupancy refined to 0.6(2), for the second molecule the occupancy was refined and then fixed at 0.2. C−N and C−C bond lengths were fixed at 1.40(5)/1.54(5) or 1.40(7)/1.54(7) Å values, respectively, by means of the corresponding DFIX restraints. For N3N/C3N, an EADP constraint was used. On the final difference Fourier map, the highest peak of 1.21 e/Å^3 is located at 1.18 Å from Pb1. Figure S3 shows the packing and molecular structure of **2.**

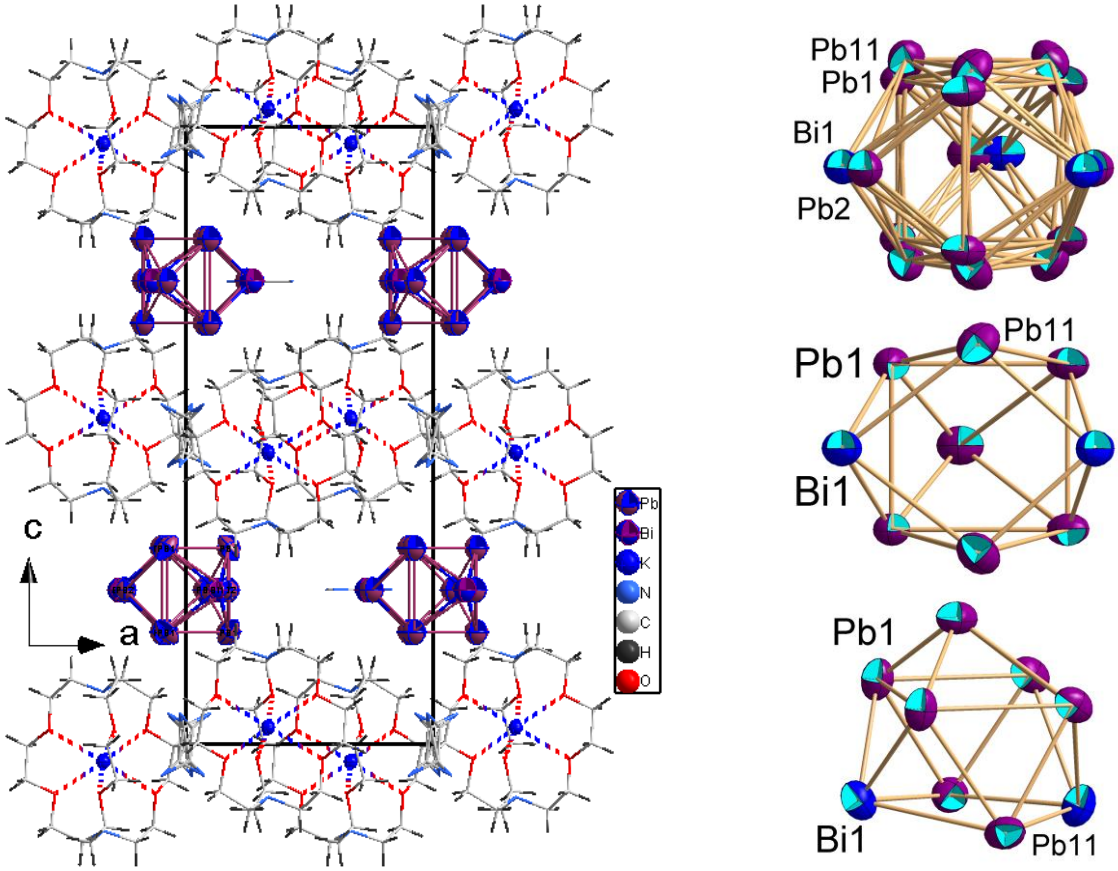

Figure S3. Packing of anions (without disorder) and cations in the crystal lattice of compound **2**, viewed along the crystallographic *b*-axis (left); illustration of the disorder (top right) and one of the possible rotational orientations in two different viewing directions (center and bottom right). Selected bonding distances within the anion [pm]: Pb/Bi−Pb 2.605(5)-3.379(4) Å.

Compound $C_{72}H_{124}Bi_5K_3N_{10}Ni_2O_{18}Pb_7$ (3): The structure of compound **3** was solved in the monoclinic space group *C*2/*c*. Pb/Bi sites in the cluster anion seem to be affected by occupational disorder. Occupancies of the Pb/Bi disorder components were refined as free variables with careful manual control using EXYZ/EADP constraints. Subsequently, the refined occupancies were constrained. ISOR restraints were applied to C25 and C15 light atoms. DFIX/anti-bumping DFIX restraints were applied to the selected interatomic distances in solvent molecules. On the final difference Fourier map, the highest peak of 1.69 e/Å^3 is located at 1.27 Å from Pb5. See Figure S4 for the packing of cations and anions in **3**.

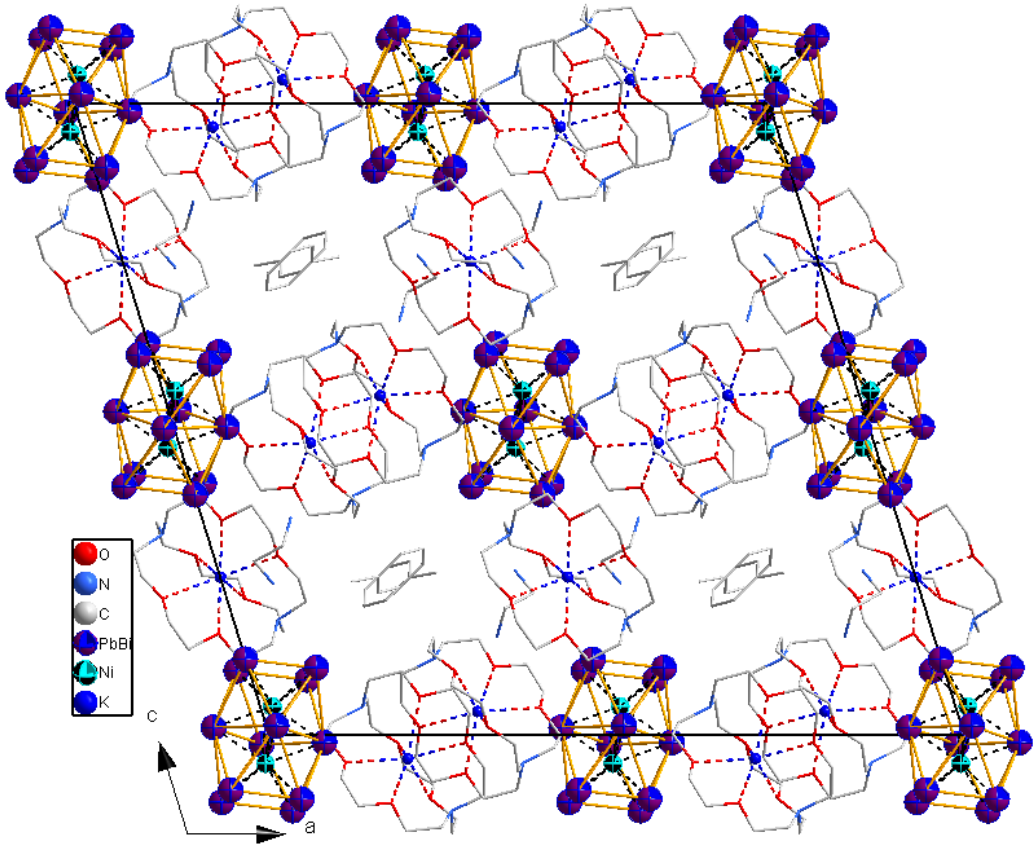

Figure S4. Packing of anions and cations in **3**, viewed along the crystallographic *b*-axis. H atoms of [2.2.2]crypt/solvent molecules are omitted for clarity. Selected distances within the anion (see Figure 2 in the main manuscript) [pm]: Pb/Bi1/2−Pb/Bi1/2 342.9(2)-337.2(3), Pb/Bi3-6−Pb/Bi3-6 305.8(2)-307.3(2), Pb/Bi1/2−Pb/Bi3-6 333.3(2)-337.7(2), Ni−Pb/Bi 269.9(3)-272.0(3), Ni−Ni 249.9(7).

Compound $C_{72}H_{144}Bi_8O_{24}K_4N_8Zn_6Pb_3$ (4): The structure of compound **4** was solved in the triclinic space group *P*−1. Problems with data quality/completeness had to be faced, which is not uncommon for the crystal structures of this class of compounds. A substitutional disorder was introduced in the pentagonal face of the $[Pb_3Bi_8Zn_6]^{4-}$ cluster, constraining the occupancies of Bi/Pb on each of the five positions at 0.4/0.6, respectively, to reflect the results of EDX and ESI-MS measurements. The overall low quality of the diffraction data for this compound made it necessary to refine the atomic positions and displacement parameters of the $[K([2.2.2]crypt)]^+$ cations using a large number of restraints to maintain reasonable values of geometric parameters. The applied restraints include ISOR, DFIX/anti-bumping DFIX for C−C, C−O, C…K, C−N bond lengths/interatomic distances. Due to the difficulties in refining the light atom part of the structure, the spurious electron densities of heavily disordered solvent molecules were extracted using the SQUEEZE[4] algorithm. On the final difference Fourier map, the highest peak of 2.94 e/Å^3 is located at 1.68 Å from Bi8. Figure S5 shows the packing of cations and anions of compound **4**, viewed along the crystallographic *c*-axis.

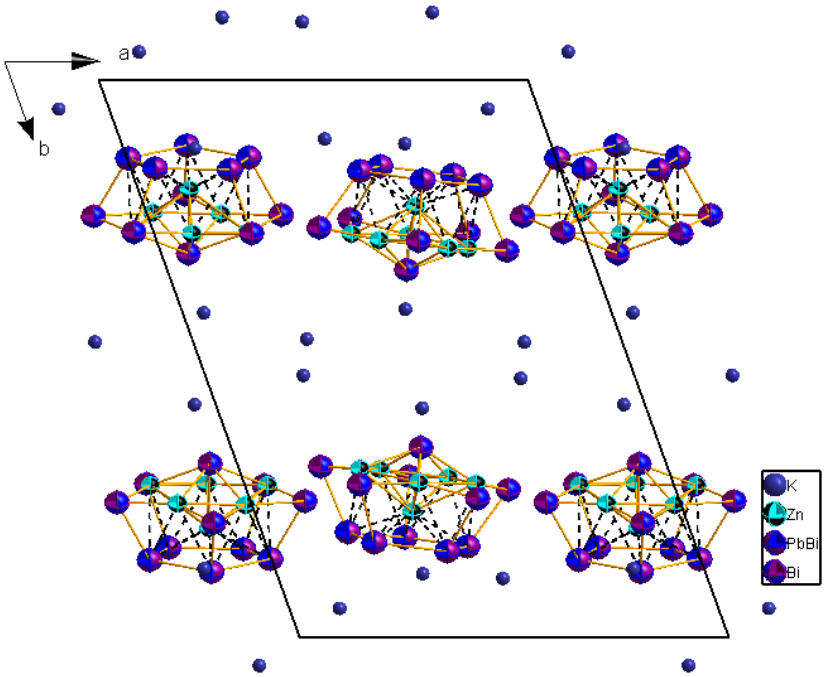

Figure S5. Packing of anions and cations in **4** viewed along the crystallographic *c*-axis. O, N, C and H atoms of the cations have been omitted for clarity. Selected distances within the anion (see Figure 2 in the main manuscript) [pm]: Bi1-5−Pb/Bi7-11 301.4(3)-306.5(3), Pb/Bi7-11−Pb/Bi7-11 313.7(3)-321.9(2), Bi1-5−Zn 268.5(5)-272.3(5), Pb/Bi7-11−Zn 318.5(6)-345.2(5), Bi6−Zn 279.0(5)-300.5(6), Zn−Zn 292.6(6)-325.4(7).

4. Electrospray Ionization Mass Spectrometry (ESI-MS) Investigations

ESI-MS has been performed on a Finnigan LTQ-FT spectrometer by Thermo Fischer Scientific in the negative ion mode: Spray voltage 3.90 kV, capillary temperature 300°C, capillary voltage –11 V, tube lens voltage –140.38 V, sheath gas flow rate 25 arb, sweep gas flow rate 0 arb.

4.1 ESI-MS Investigations of binary Pb/Bi anions

Investigation in ethane-1,2-diamine (en, positive ion mode): For *en* solutions of the as-prepared $K(Pb,Bi)_2$ phase, an ESI-MS spectrum was recorded in positive ion mode after 3 hours (Figure S6). The most prominent peaks belong to the $[Bi_2]^-/[Pb_1Bi_1]^-$ mixture at m/z = 416.95 and 417.96 (not shown in Figure S6). At relative intensities of up to 3%, one can assign higher m/z signals to different kinds of species with 9 or 10 atoms. Apparently, in this solvent the original cages undergo fragmentation and re-organization into other species; this may be due to an intrinsic dynamic process in solution, or to the harsh ESI-MS conditions.

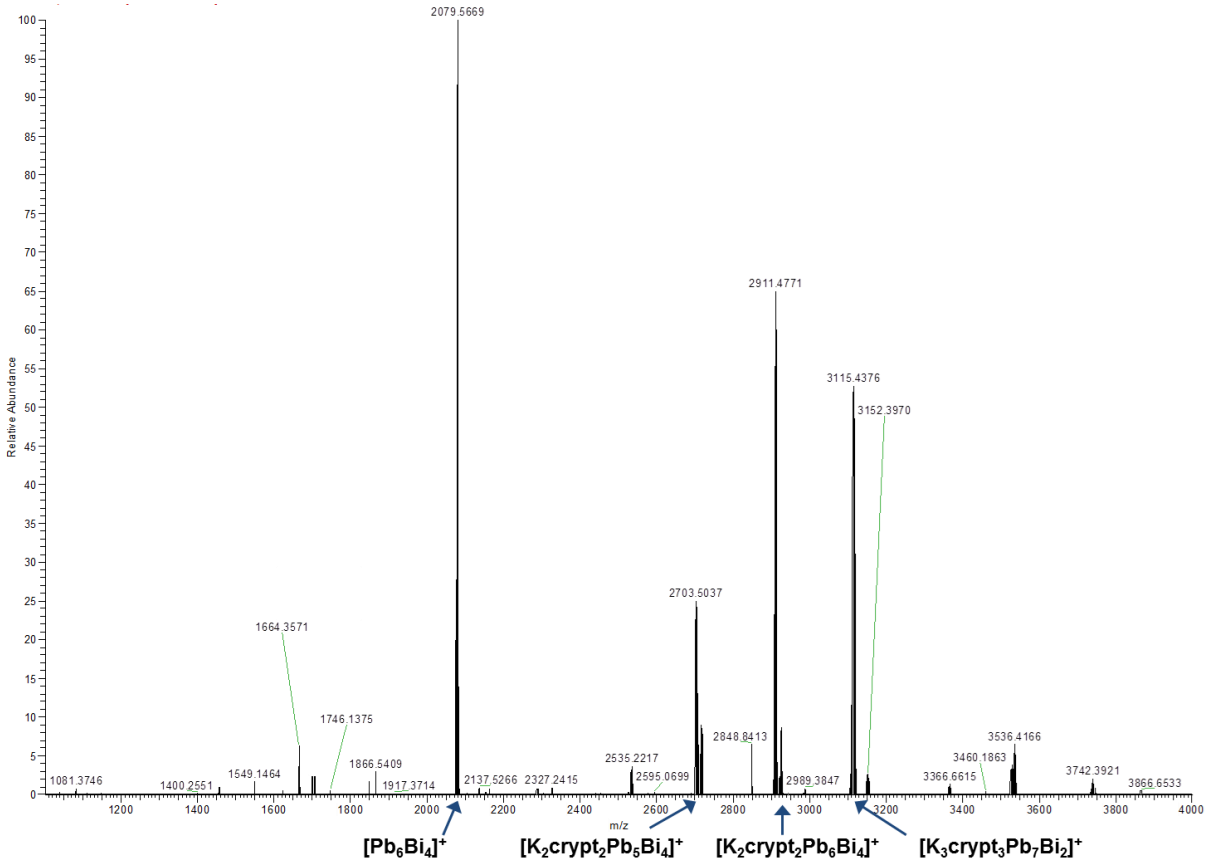

Figure S6. Overview ESI mass spectrum recorded from a solution of the as-prepared $K(Pb,Bi)_2$ phase in *en* (positive ion more) with assignment of identifiable signals. Note that the intensity of the most prominent peak at m/z = 2079.5669 is only 3% of the 100% intensity signal of the $[Bi_2]^-/[Pb_1Bi_1]^-$ mixture at m/z = 416.95 and 417.96, which are not shown here.

Figure S7 - Figure S10 show zooms of identifiable peaks:

at m/z = 2079.56; 10-atom fragment $[Pb_6Bi_4]^+$

at m/z = 2703.50; 9-atom fragment $[K_2crypt_2Pb_5Bi_4]^+$

at m/z = 2911.47; 10-atom fragment $[K_2crypt_2Pb_6Bi_4]^+$

at m/z = 3115.43; 9-atom fragment $[K_2crypt_3Pb_7Bi_2]^+$

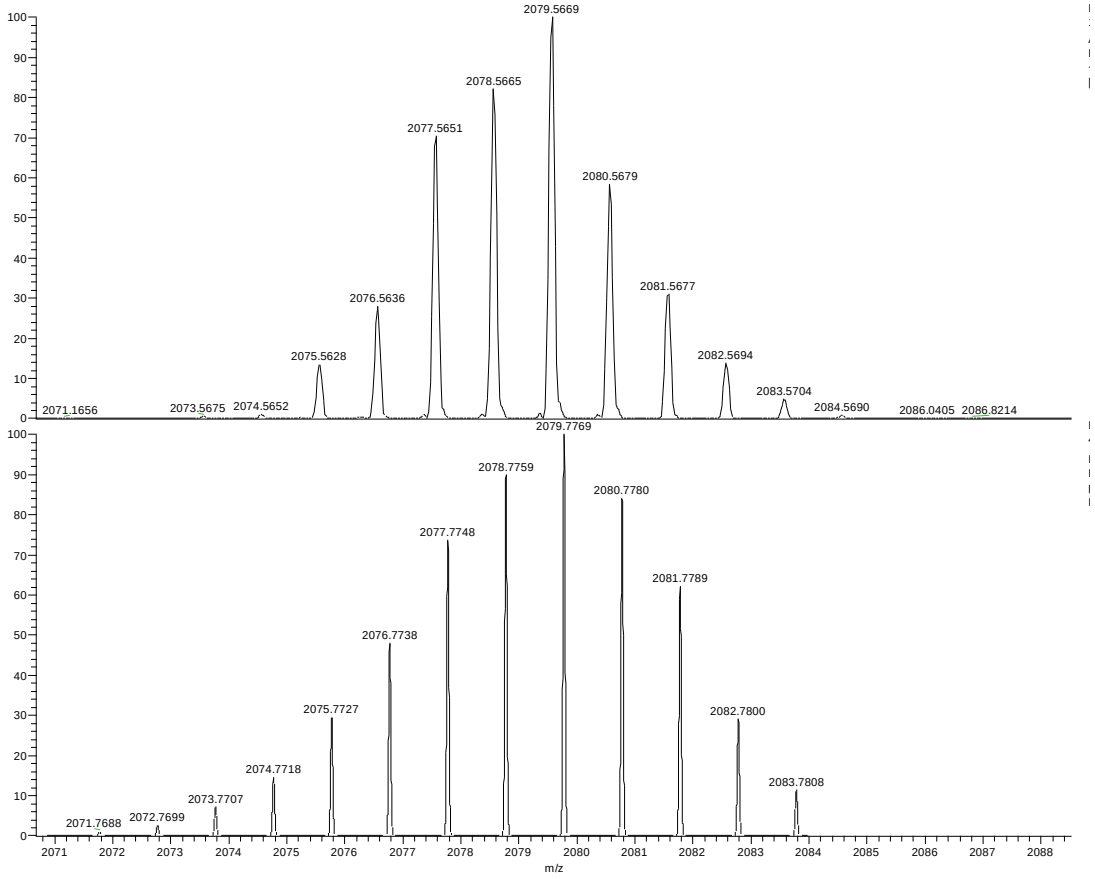

Figure S7. Measured (top) and simulated (bottom) spectrum of the fragment $[Pb_6Bi_4]^+$.

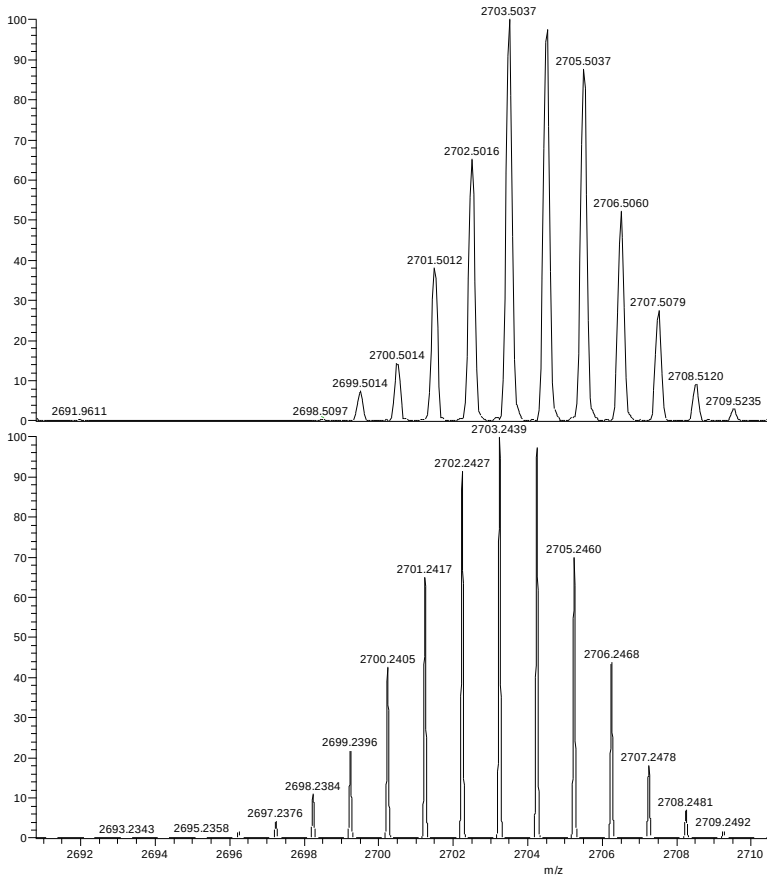

Figure S8. Measured (top) and simulated (bottom) spectrum of the fragment $[K_2(crypt)_2Pb_5Bi_4]^+$.

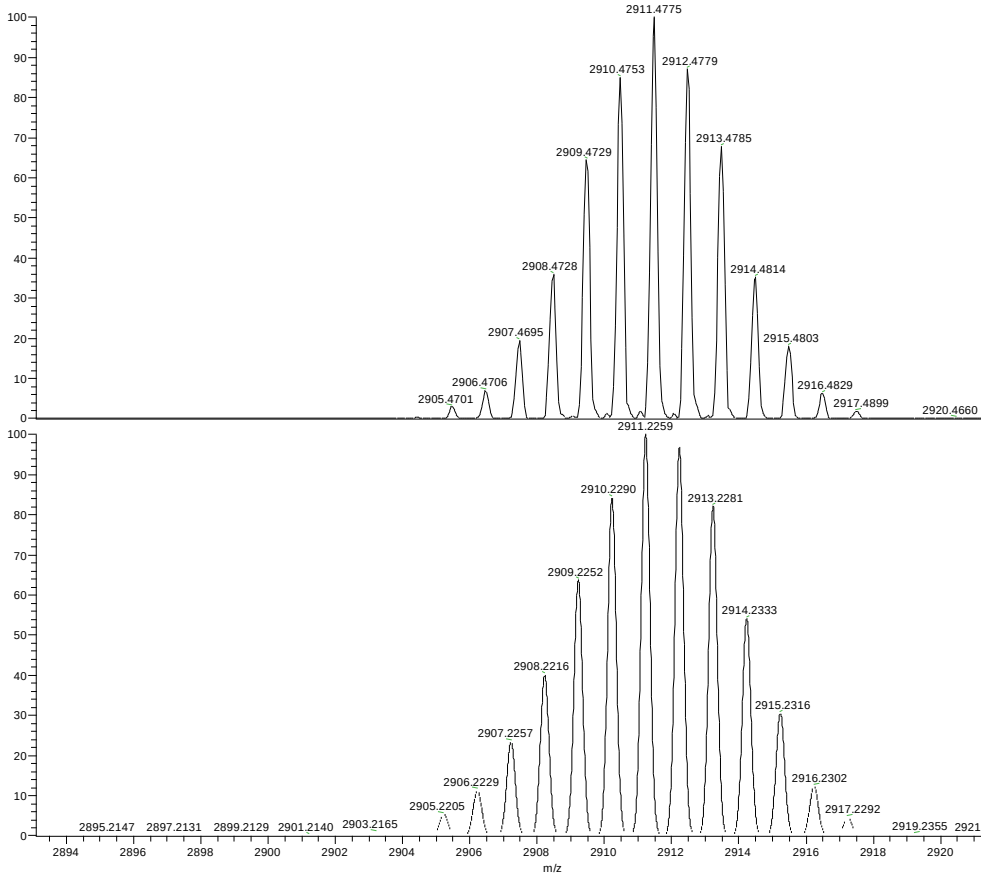

Figure S9. Measured (top) and simulated (bottom) spectrum of the fragment $[K_2(crypt)_2Pb_6Bi_4]^+$.

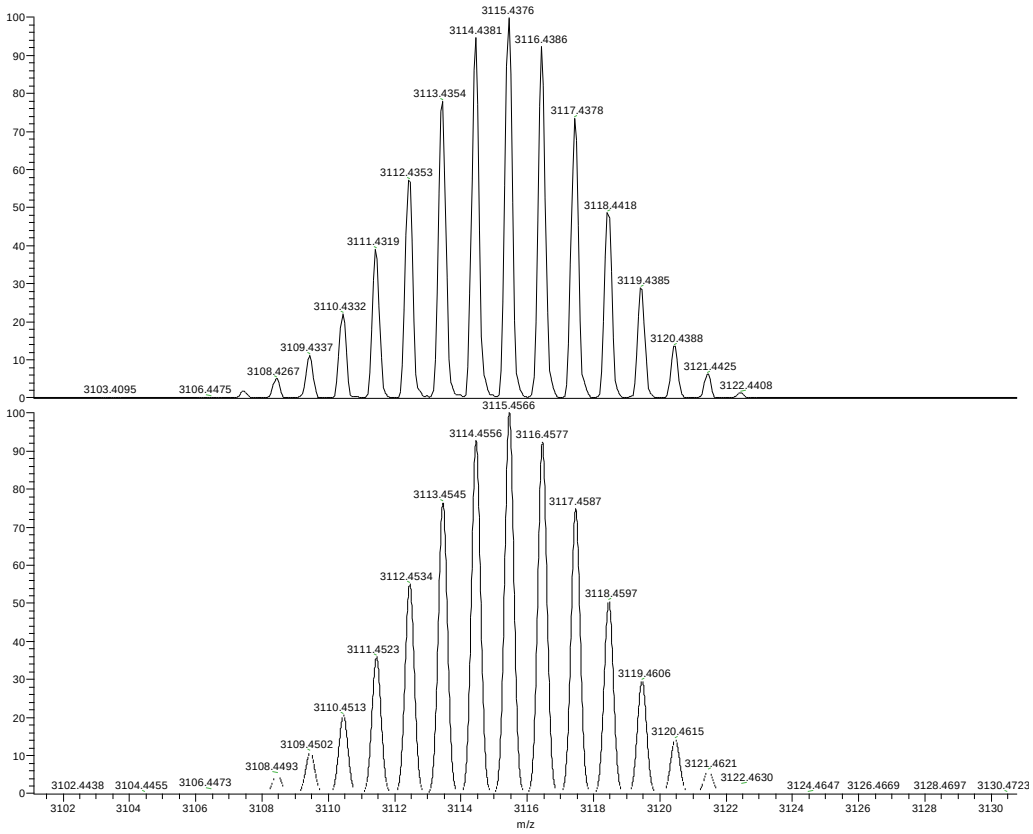

Figure S10. Measured (top) and simulated (bottom) spectrum of the fragment $[K_3(crypt)_3Pb_7Bi_2]^+$.

Investigations in the negative ion mode were performed on both $K(Pb,Bi)_2$ and single-crystals of **1**. These are identical and also show fragmentation (Figure S11). Here, the most prominent signal derives from a four-atom cage $[Pb_1Bi_3]^-$ at m/z = 834.9180, being followed by the $[Bi_2]^-/[Pb_1Bi_1]^-$ mixture at m/z = 416.96 and 417.96. At higher masses, one observes 8-atom and 9-atom fragments, also under attachment of K([2.2.2]crypt). The m/z region in between is covered with signal from species that contain fragments of the organic cryptand molecules, and which have therefore not been assignable. Clearly, the fragmentation of the precursor is visible in *en* and explains the possibility or reorganization into compound **2**, **3** and **4**.

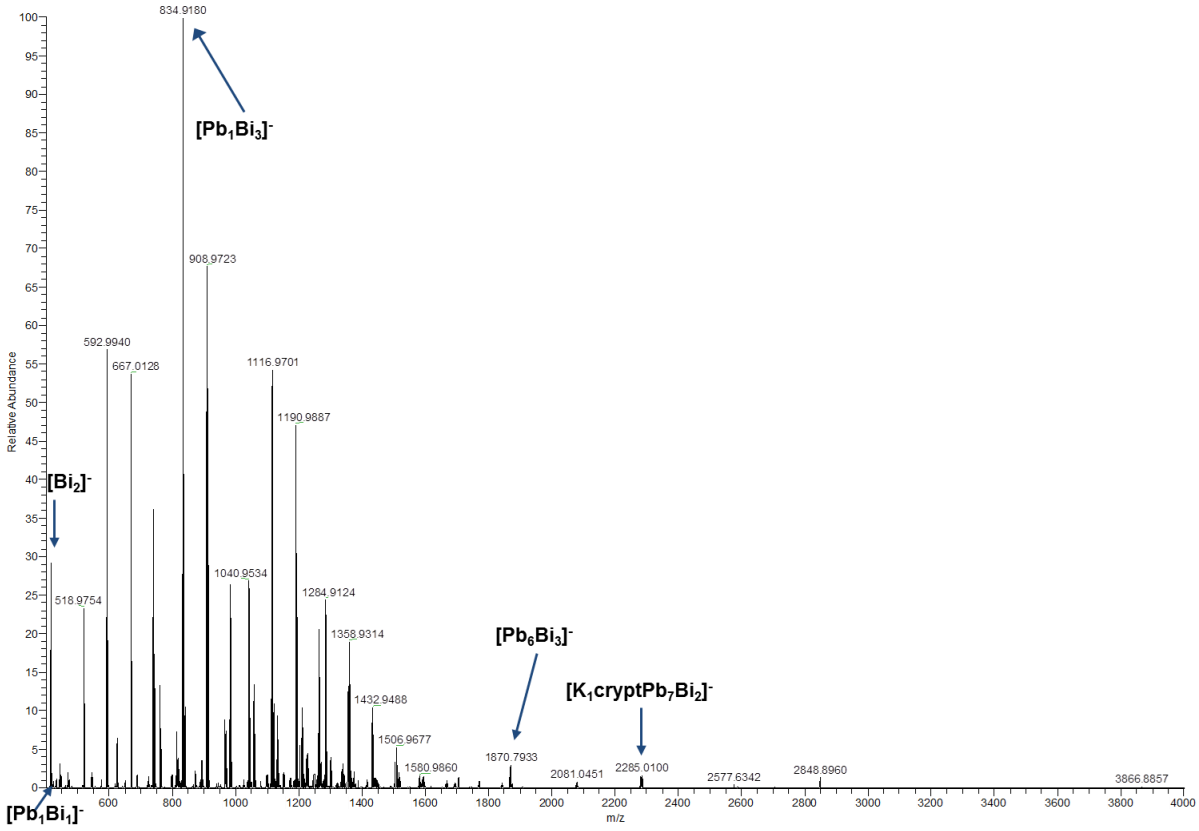

Figure S11. Overview ESI mass spectrum recorded from a solution of single-crystals of **1** in *en* (negative ion mode) with assignment of identifiable peaks. Similar results are obtained from *en* solutions of the as-prepared $K(Pb,Bi)_2$ phase.

Figure S12 - Figure S15 show zooms of identifiable peaks:

at m/z = 416.96; 2-atom fragment $[Pb_1Bi_1]^-$

at m/z = 417.96; 2-atom fragment $[Bi_2]^-$

at m/z = 834.92; 4-atom fragment $[Pb_1Bi_3]^-$

at m/z = 1870.79; 9-atom fragment $[Pb_6Bi_3]^-$

at m/z = 2855.01; 9-atom fragment $[K_1crypt_1Pb_7Bi_2]^-$

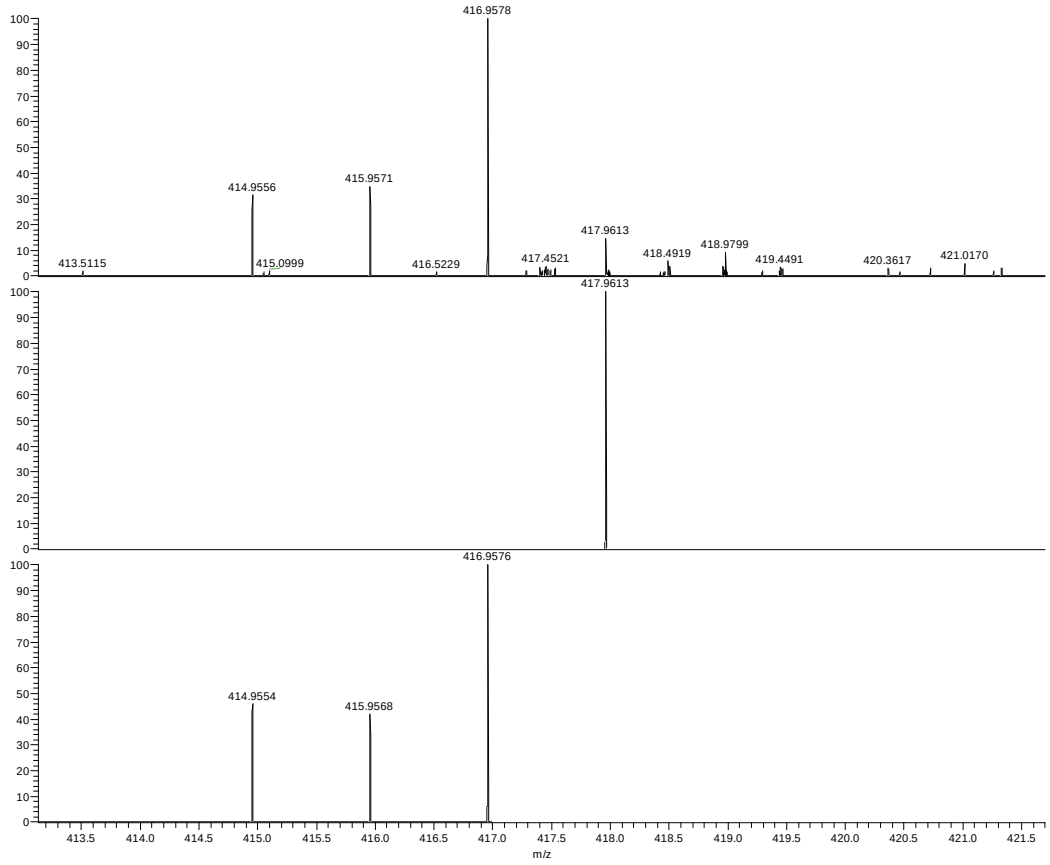

Figure S12. Measured (top) and simulated (center and bottom) spectrum of the fragments (from top) $[Bi_2]^-$ and $[Pb_1Bi_1]^-$.

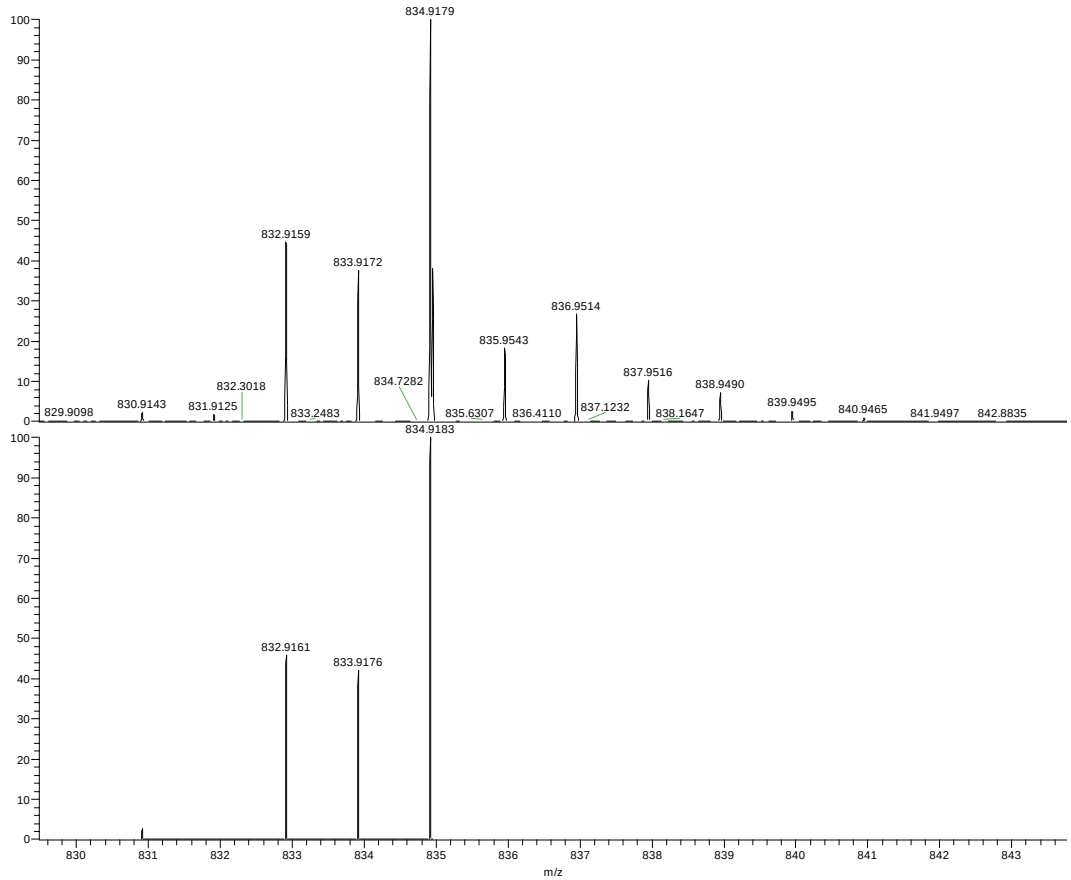

Figure S13. Measured (top) and simulated (bottom) spectrum of the fragment $[Pb_1Bi_3]^-$.

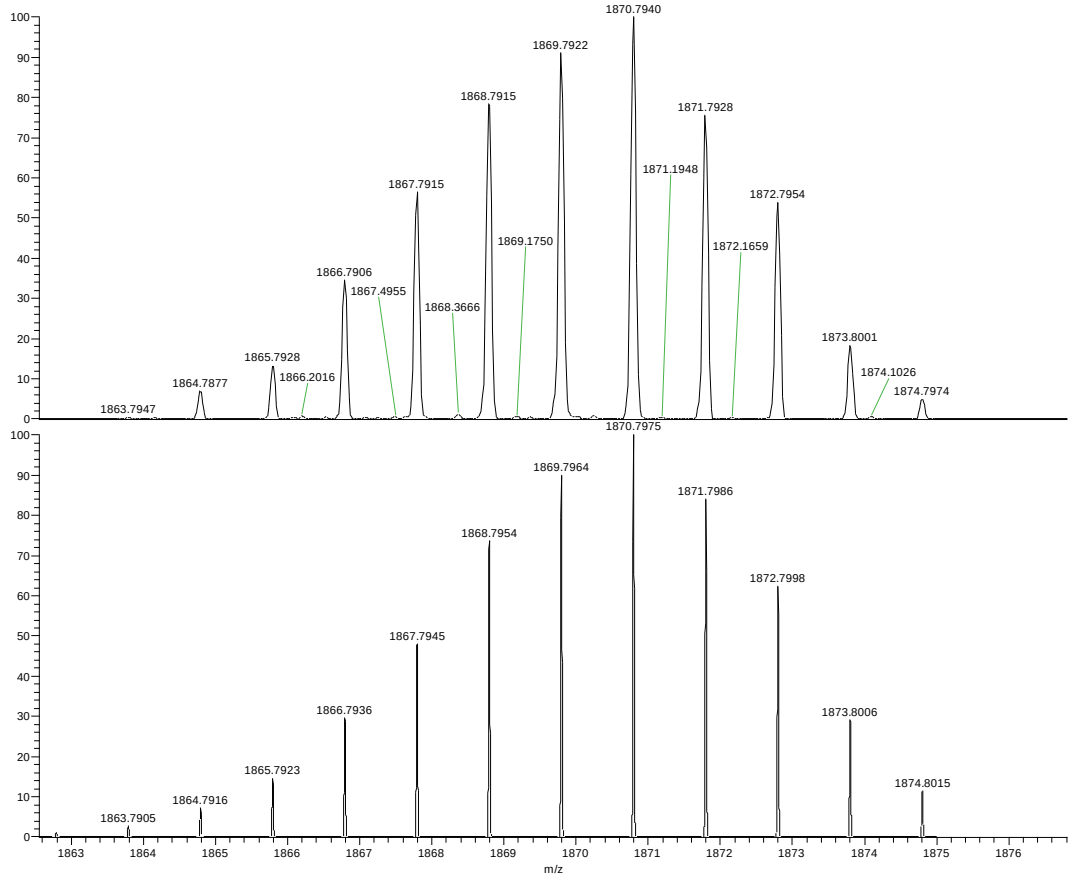

Figure S14. Measured (top) and simulated (bottom) spectrum of the fragment $[Bi_6Pb_3]^-$.

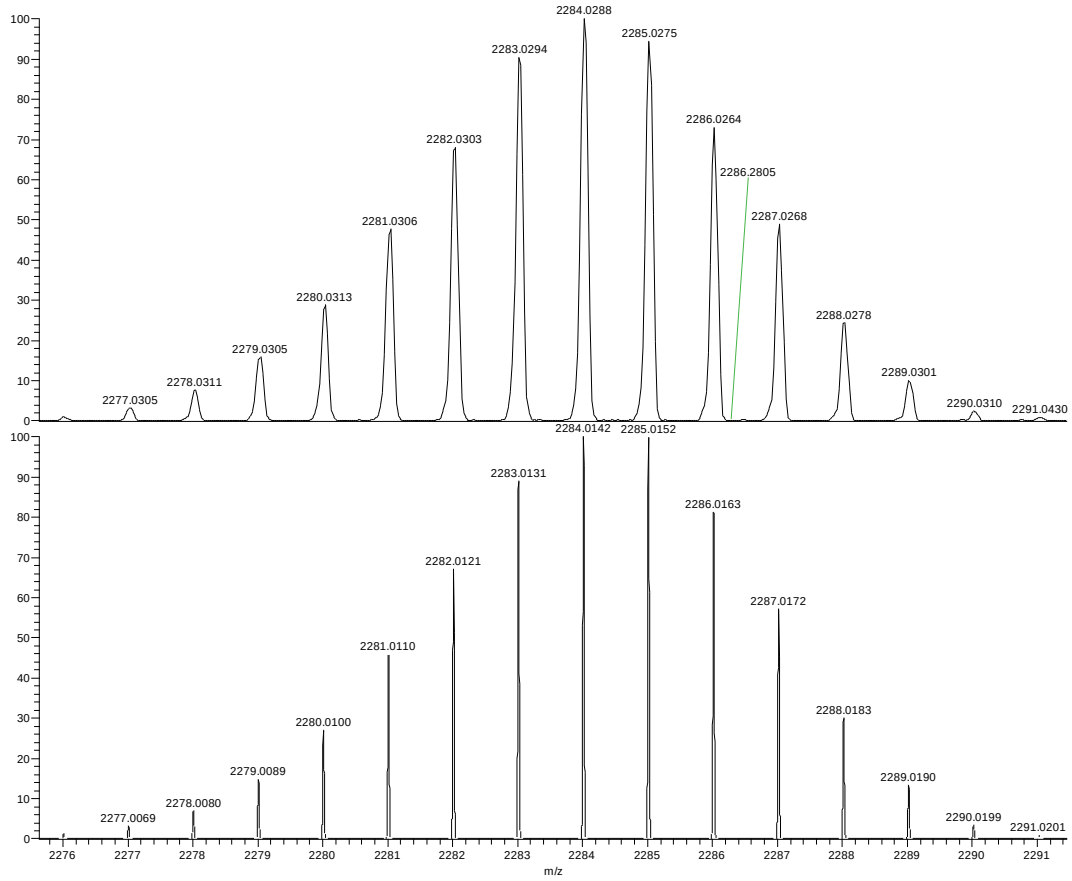

Figure S15. Measured (top) and simulated (bottom) spectrum of the fragment $[K_1cryptPb_7Bi_2]^-$

Investigations in dimethylformamide (DMF, negative ion mode): The overview ESI mass spectrum in negative mode, recorded immediately upon injection of a fresh solution of hand-selected single crystals of **1** in DMF, is provided in Figure S16. As for solutions in *en*, the ESI mass spectra indicate a fragmentation of the material and formation of other species. However, the fragmentation pattern is different from that observed in *en*; several molecular peaks appeared at the heaviest mass section 1800 – 2350 m/z that indicate the presence of Pb/Bi 9-atom cages. Also, the protonated form $[Pb_7Bi_2H]^-$ and $[K_1crypt_1Pb_7Bi_2]^-$ were detected in a small concentration. Many different fragments of lower m/z values are also present, that could be assigned to species with 2 – 8 atoms (Figure S17 - Figure S27). Due to the low intensity of many peaks, the most abundant mass (the most frequent isotopic distribution) has been used for comparison of measured and calculated peaks.

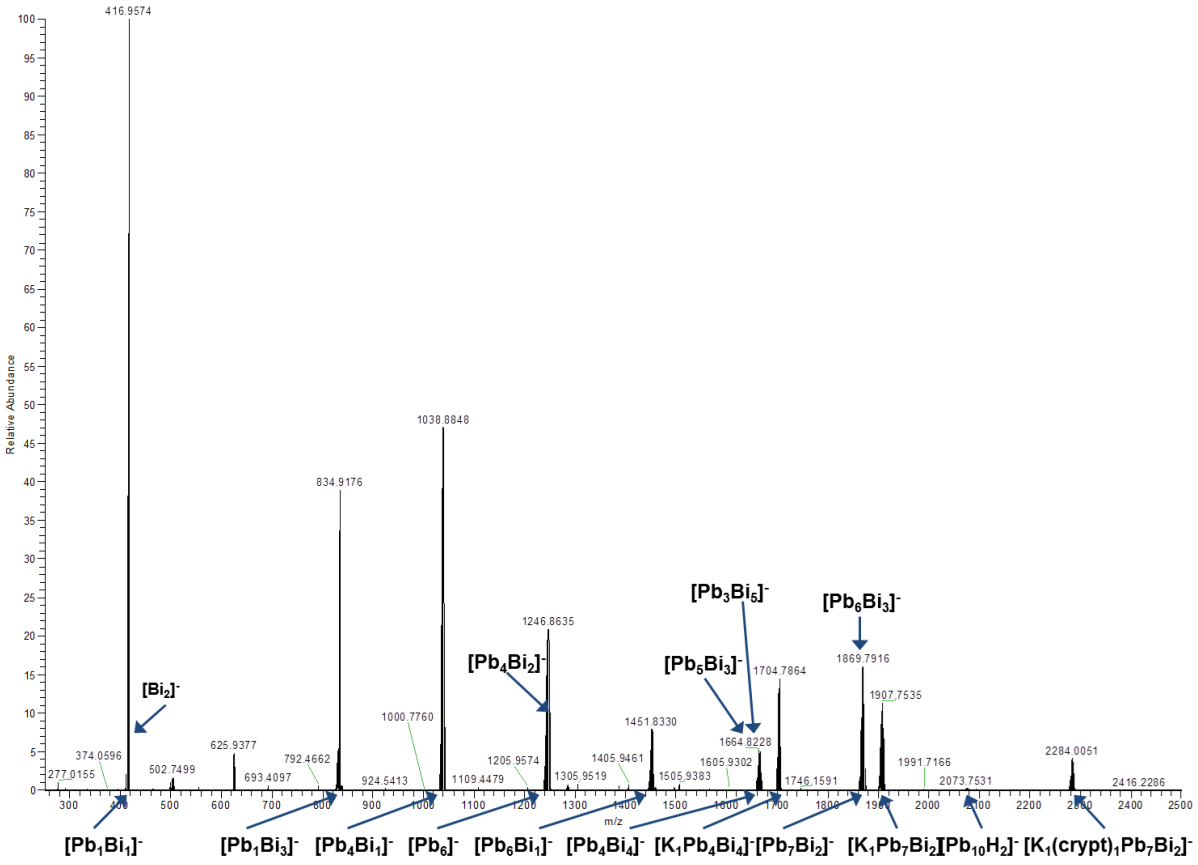

Figure S16. Overview ESI mass spectrum recorded from a solution of single-crystals of **1** in *DMF* with assignment of the most prominent peaks.

Figure S17 - Figure S27 show zooms of identifiable peaks:

at m/z = 416.95; 2-atom fragment $[Pb_1Bi_1]^-$

at m/z = 417.96; 2-atom fragment $[Bi_2]^-$

at m/z = 834.92; 4-atom fragment $[Pb_1Bi_3]^-$

at m/z = 1038.89; 5-atom fragment $[Pb_4Bi_1]^-$

at m/z = 1243.86; 6-atom fragment $[Pb_6]^-$

at m/z = 1246.86; 6-atom fragment $[Pb_4Bi_2]^-$

at m/z = 1451.83; 7-atom fragment $[Pb_6Bi_1]^-$

at m/z = 1662.82; 8-atom fragment $[Pb_5Bi_3]^-$

at m/z = 1665.82; 8-atom fragment $[Pb_4Bi_4]^-$

at m/z = 1666.82; 8-atom fragment $[Pb_3Bi_5]^-$

at m/z = 1704.78; 8-atom fragment $[K_1Pb_4Bi_4]^-$

at m/z = 1868.80; 9-atom fragment $[Pb_7Bi_2]^-$

at m/z = 1870.80; 9-atom fragment $[Pb_6Bi_3]^-$

at m/z = 1907.75; 9-atom fragment $[K_1Pb_7Bi_2]^-$

at m/z = 2074.77; 10-atom fragment $[Pb_{10}H_2]^-$ (trace)

at m/z = 2285.00; 9-atom fragment $[K_1crypt_1Pb_7Bi_2]^-$

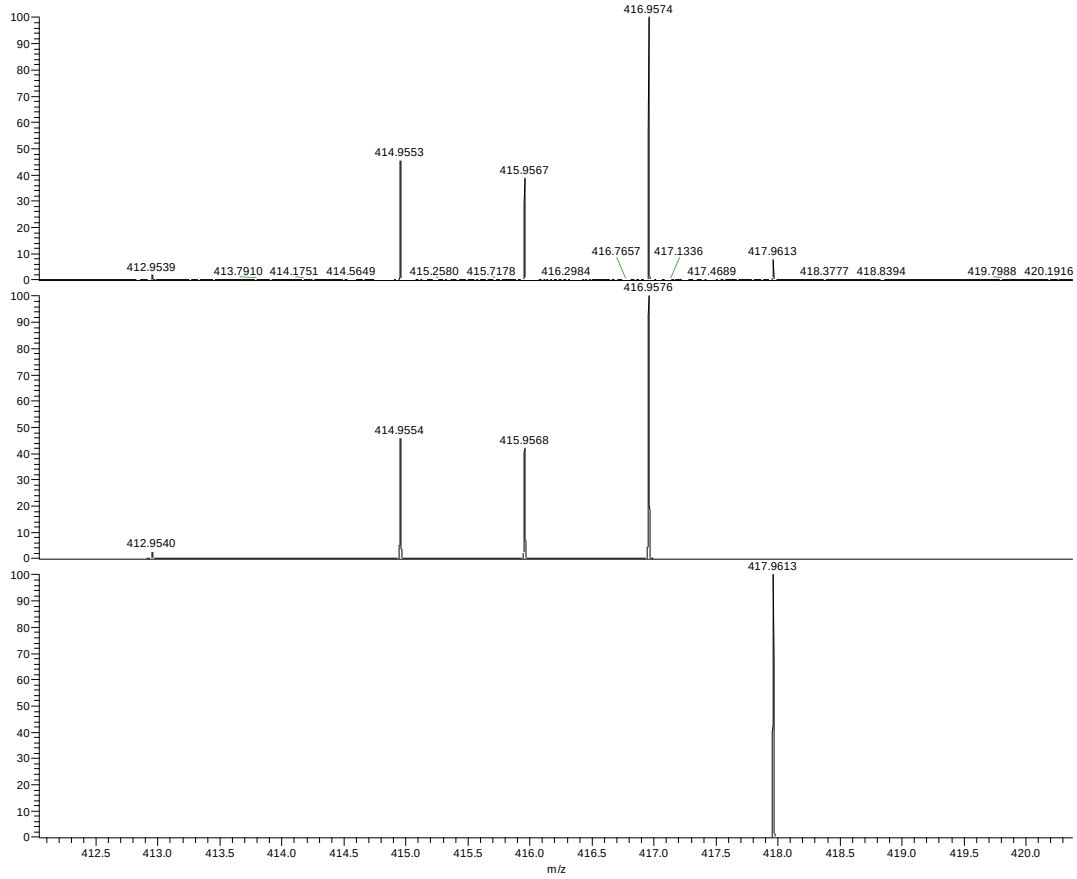

Figure S17. Measured (top) and simulated (center and bottom) spectrum of the fragments (from top) $[Pb_1Bi_1]^-$ and $[Bi_2]^-$.

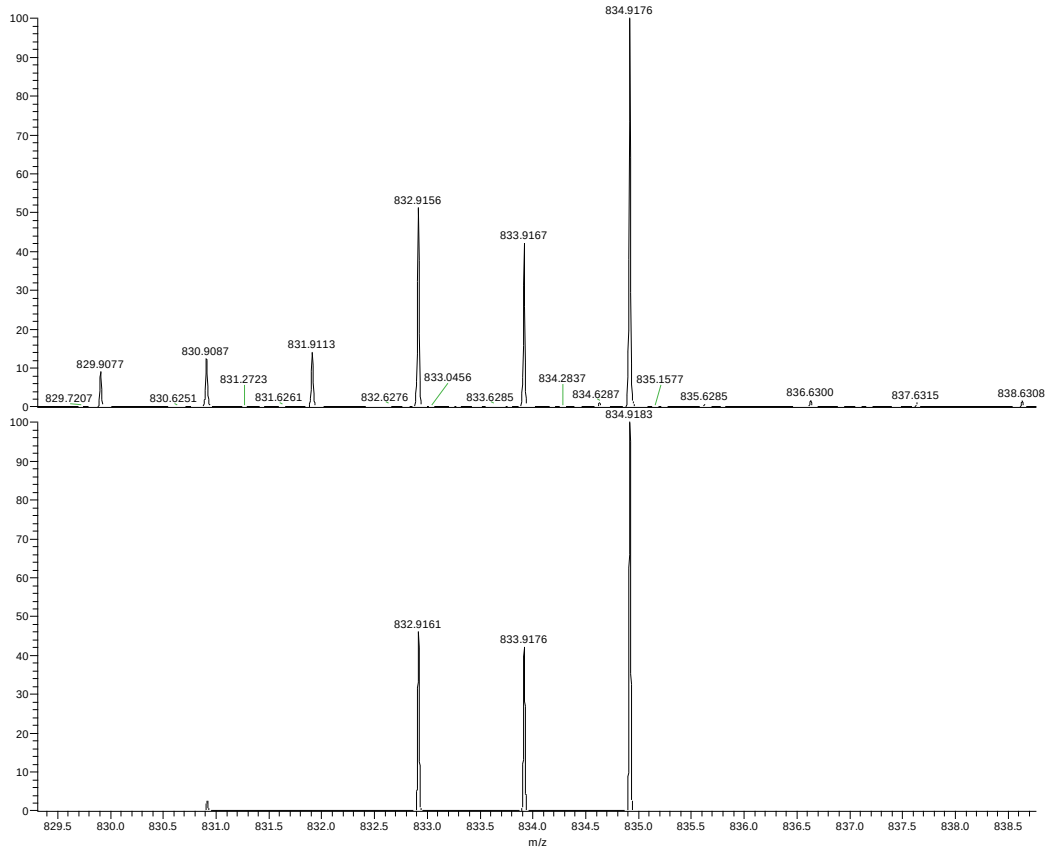

Figure S18. Measured (top) and simulated (bottom) spectrum of the fragment $[Pb_1Bi_3]^-$.

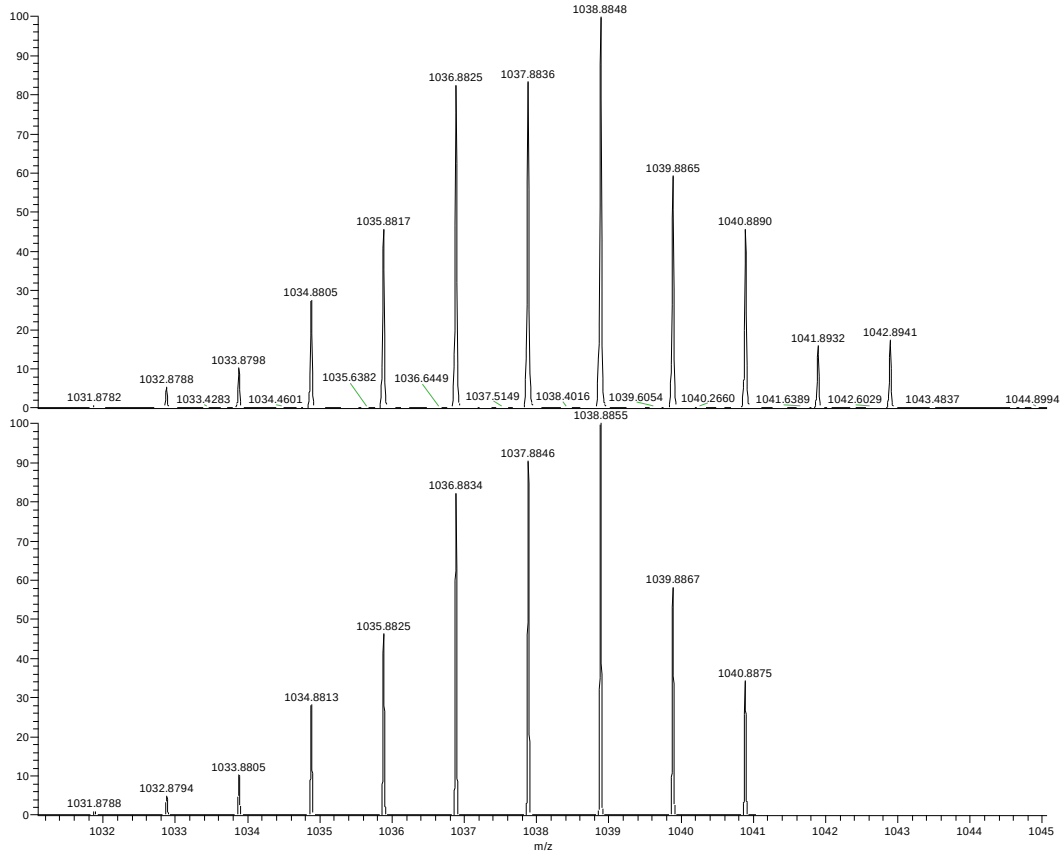

Figure S19. Measured (top) and simulated (bottom) spectrum of the fragment $[Pb_4Bi_1]^-$.

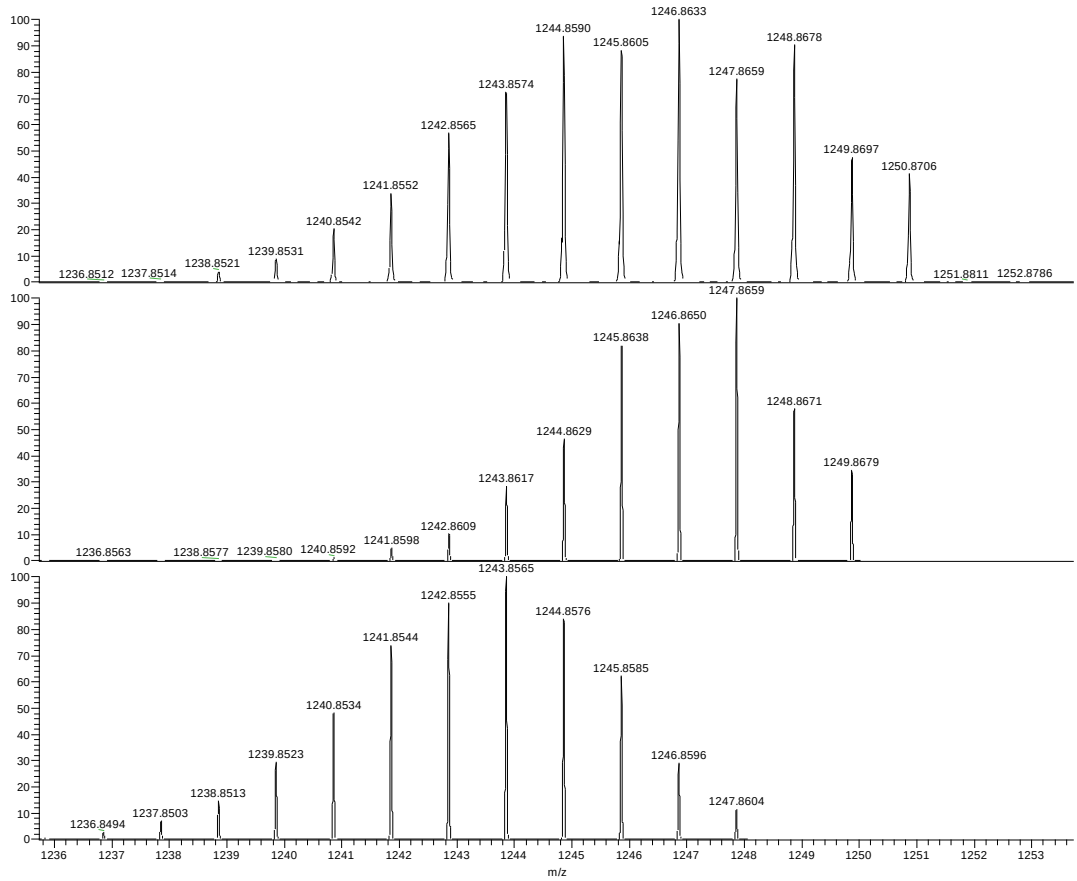

Figure S20. Measured (top) and simulated (center and bottom) spectrum of the fragments (from top) $[Pb_4Bi_2]^-$ and $[Pb_6]^-$.

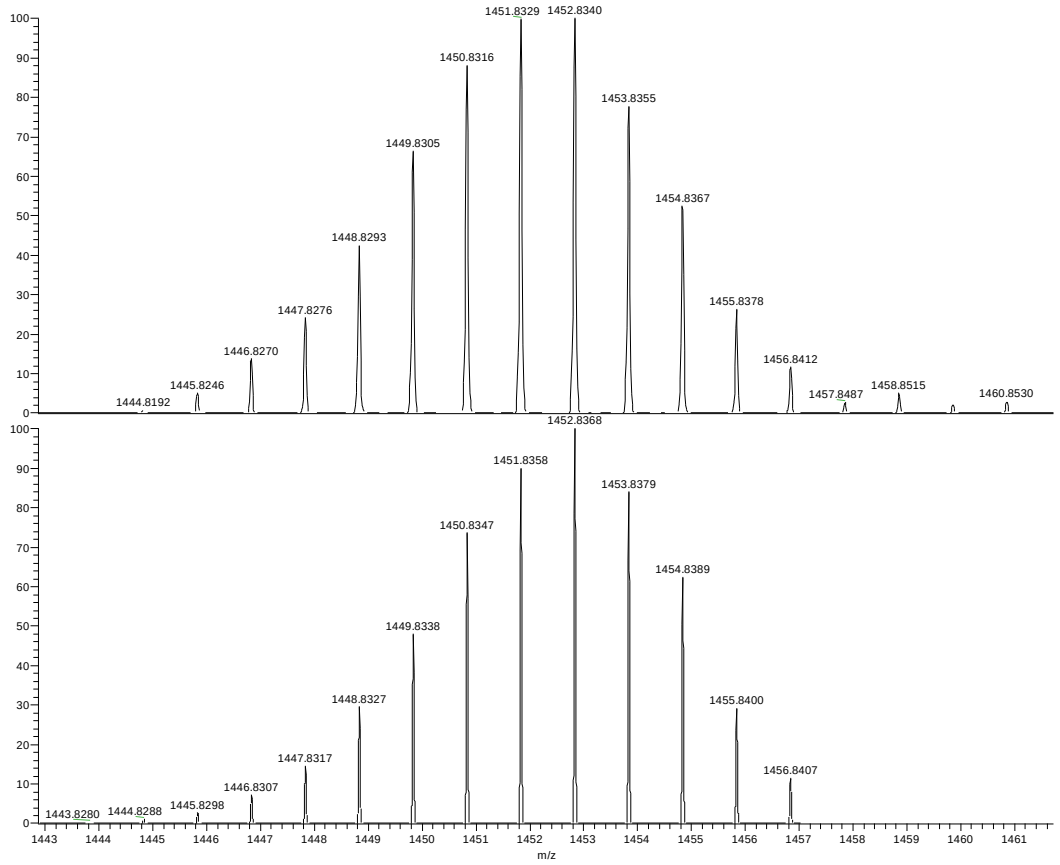

Figure S21. Measured (top) and simulated (bottom) spectrum of the fragment $[Pb_6Bi_1]^-$.

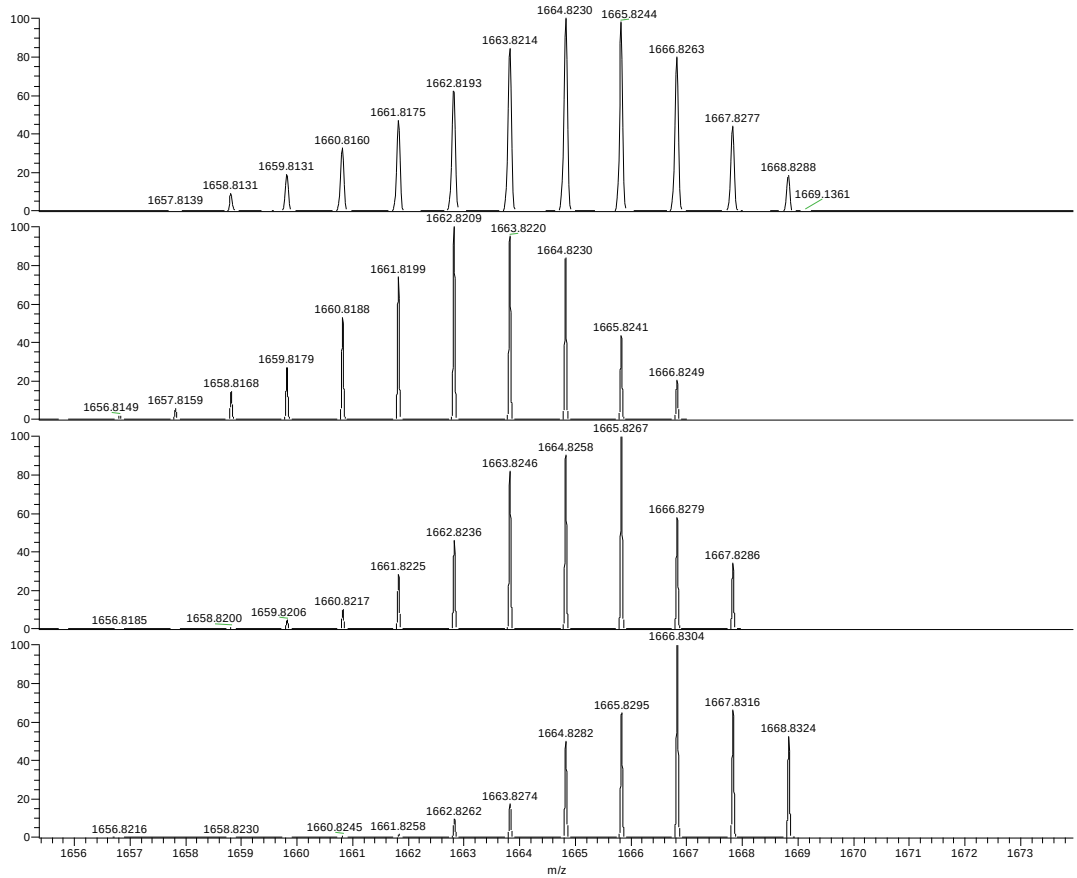

Figure S22. Measured (top) and simulated (centers and bottom) spectrum of the fragments (from top) $[Pb_5Bi_3]^-$, $[Pb_4Bi_4]^-$ and $[Pb_3Bi_5]^-$.

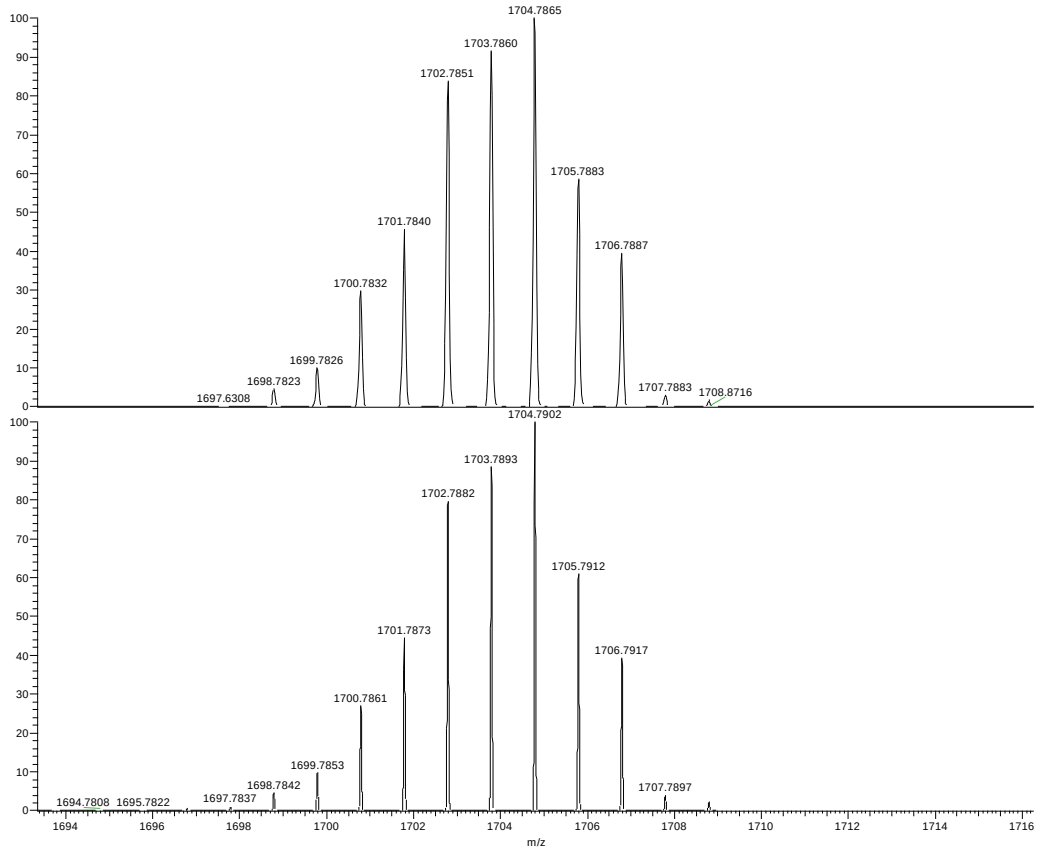

Figure S23. Measured (top) and simulated (bottom) spectrum of the fragment $[K_1Pb_4Bi_4]^-$.

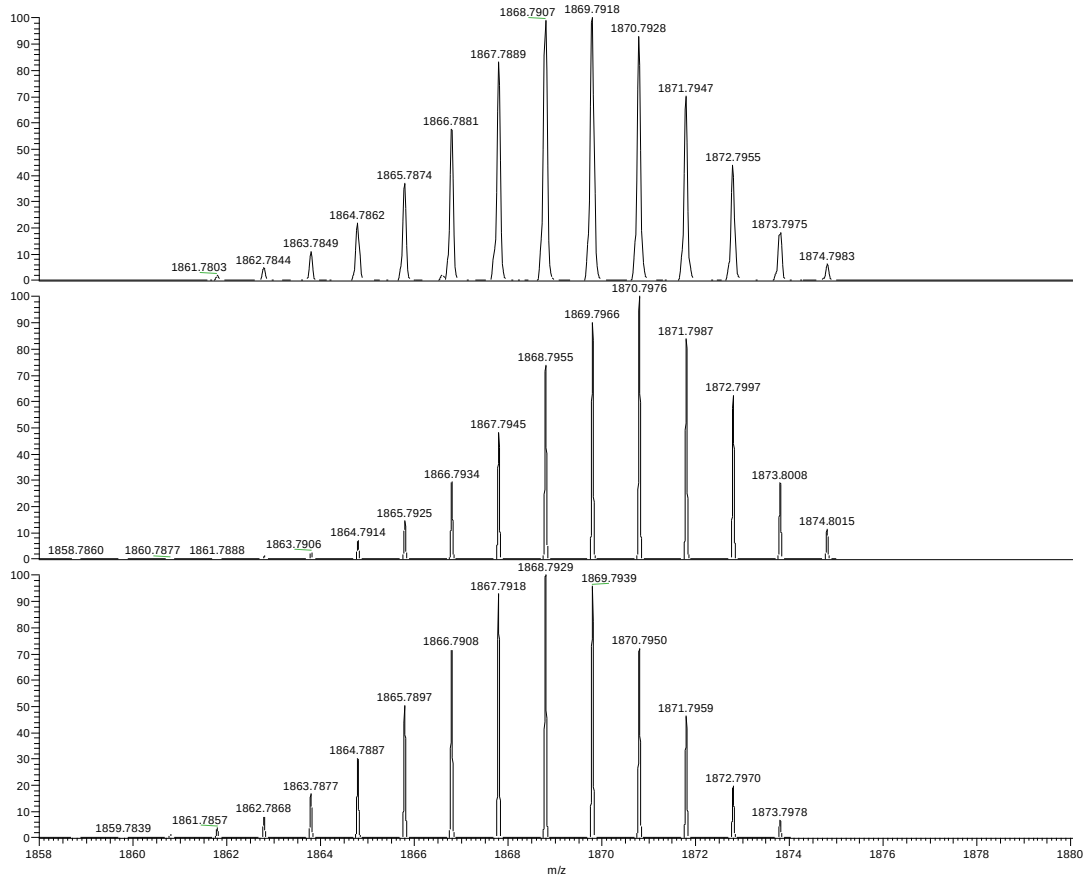

Figure S24. Measured (top) and simulated (center and bottom) spectrum of the fragments (from top) $[Pb_6Bi_3]^-$ and $[Pb_7Bi_2]^-$.

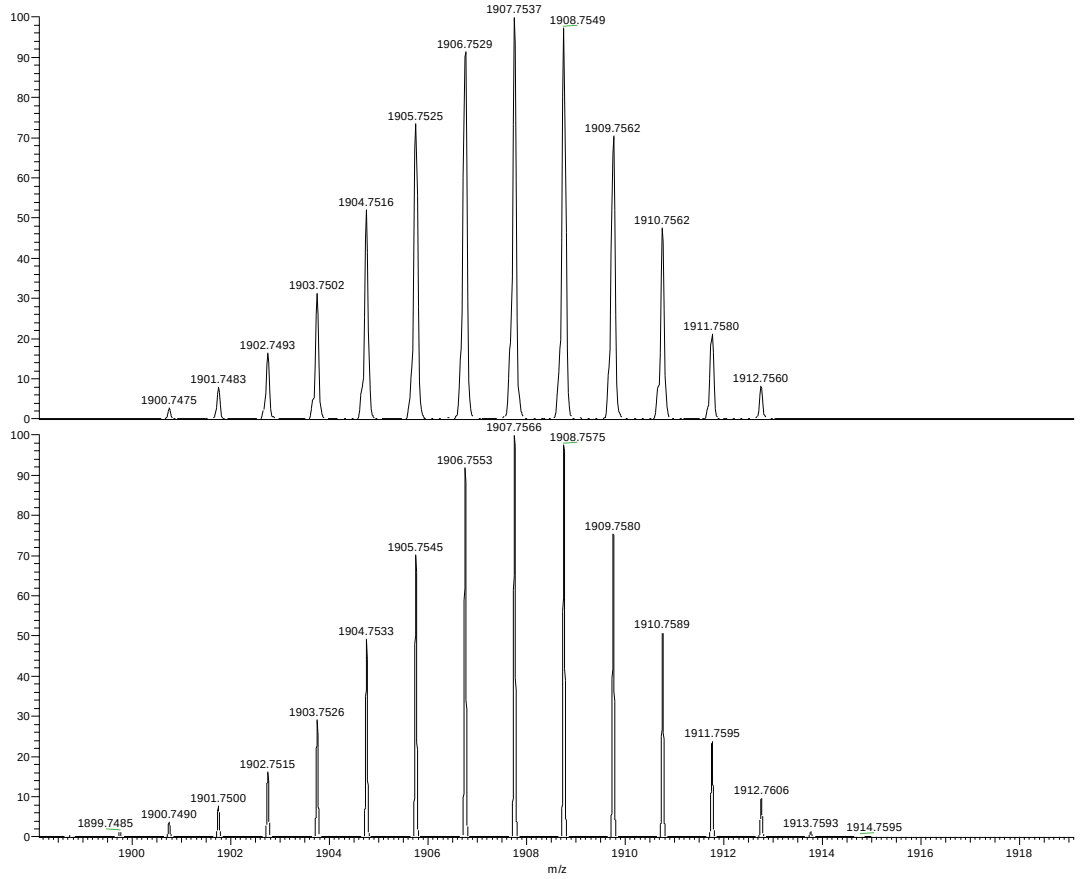

Figure S25. Measured (top) and simulated (bottom) spectrum of the fragment $[K_1Pb_7Bi_2]^-$.

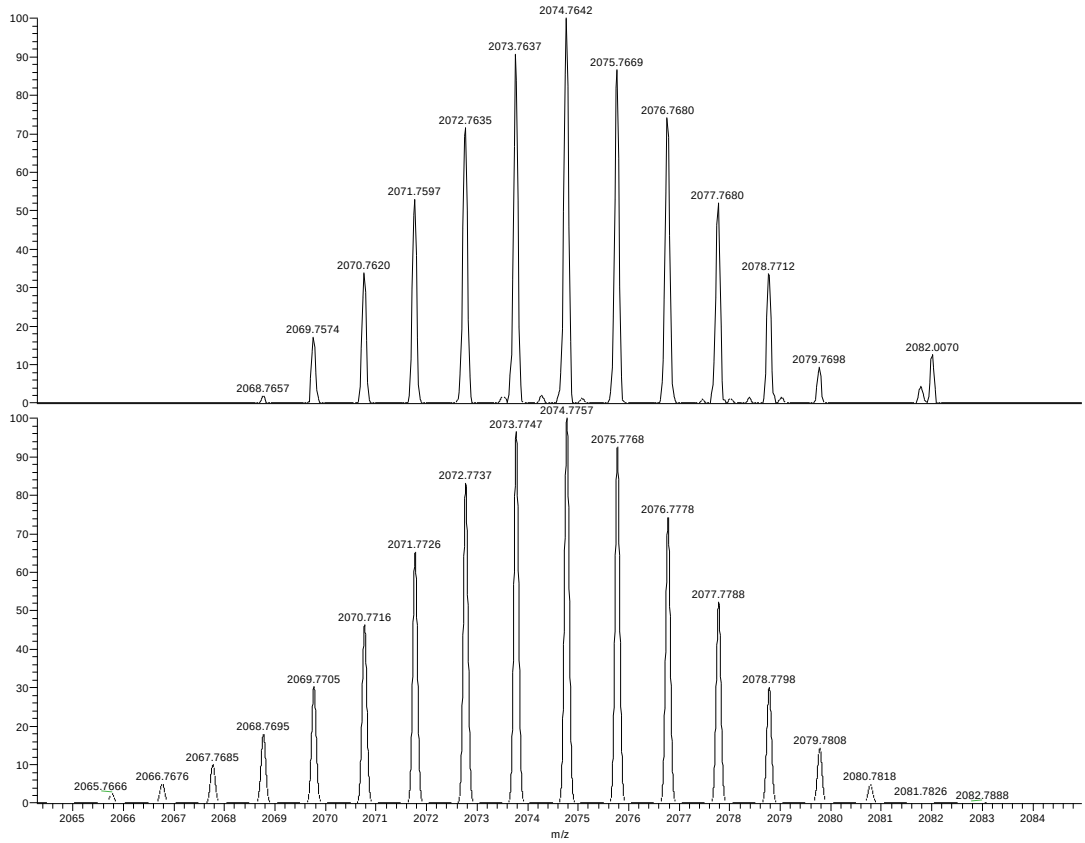

Figure S26. Measured (top) and simulated (bottom) spectrum of the fragment $[Pb_{10}H_2]^-$.

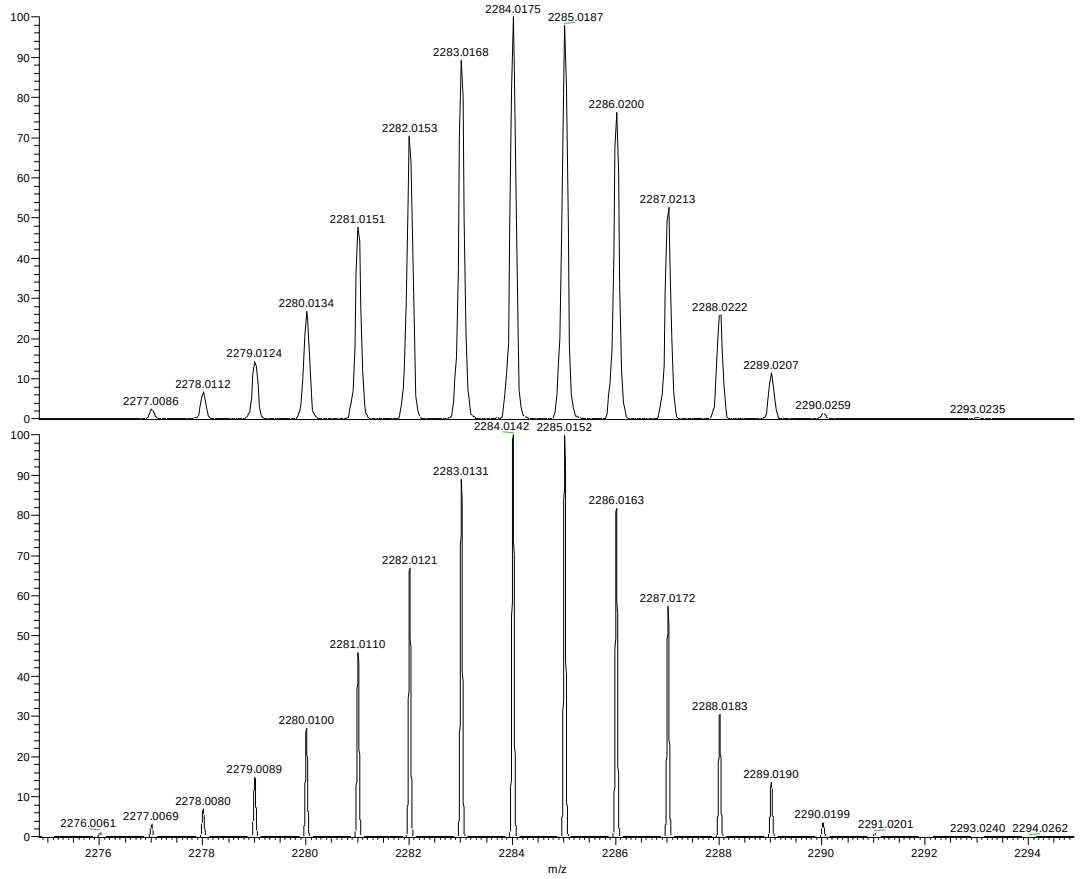

Figure S27. Measured (top) and simulated (bottom) spectrum of the fragment $[K_1(crypt)_1Pb_7Bi_2]^-$.

4.2 ESI-MS Investigations of crystals of 3 and 4 in DMF

General: Crystals of **3** and **4** have been dissolved in DMF at room temperature and immediately injected. It was not possible to record ESI-MS spectra of the compounds in *en* solution, since the single-crystals decomposed to produce amorphous powder instead of dissolving.

Investigation of compound 3: Most predominant and significant peaks characteristic to cluster **3** − in agreement with EDX and the crystal structure analysis − are present in the higher m/z region, and demonstrate a fairly good stability (Figure S28). The formation of an $[Ni_1Pb_6Bi_3]^-$ fragment may be the result of the dissolution of the single crystals in DMF, or may have been due to the ESI conditions. A zoom into the molecular peak of all species is provided in the main manuscript (Figure 3).

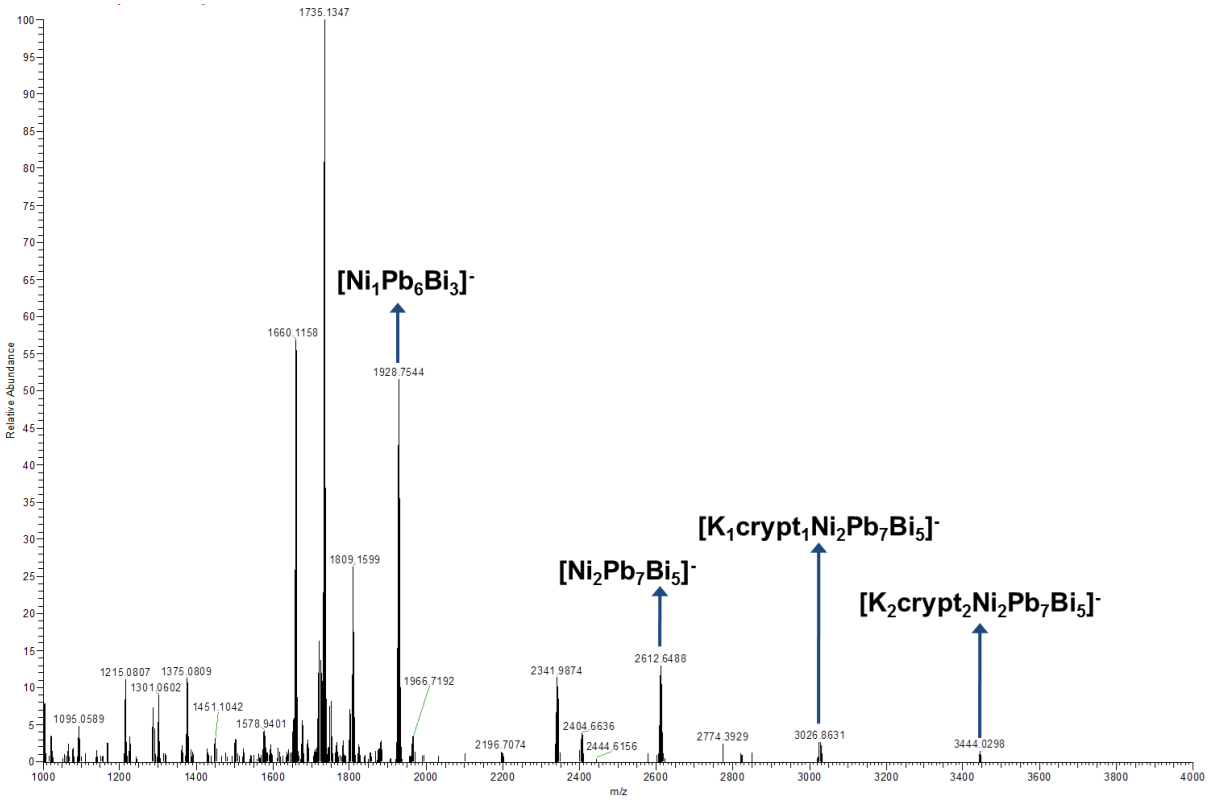

Figure S28. Overview ESI mass spectrum, recorded immediately upon injection of a fresh solution of hand-selected single crystals of **3** in DMF.

Figure S29 - Figure S32 show zooms of identifiable peaks of **3**:

at m/z = 1928.75; ten-atom fragment $[Ni_1Pb_6Bi_3]^-$

at m/z = 2612.64; fourteen-atom fragment $[Ni_2Pb_7Bi_5]^-$

at m/z = 3026.86; fourteen-atom fragment $[K_1crypt_1Ni_2Pb_7Bi_5]^-$

at m/z = 3115.43; fourteen-atom fragment $[K_2crypt_2Pb_7Bi_5]^-$

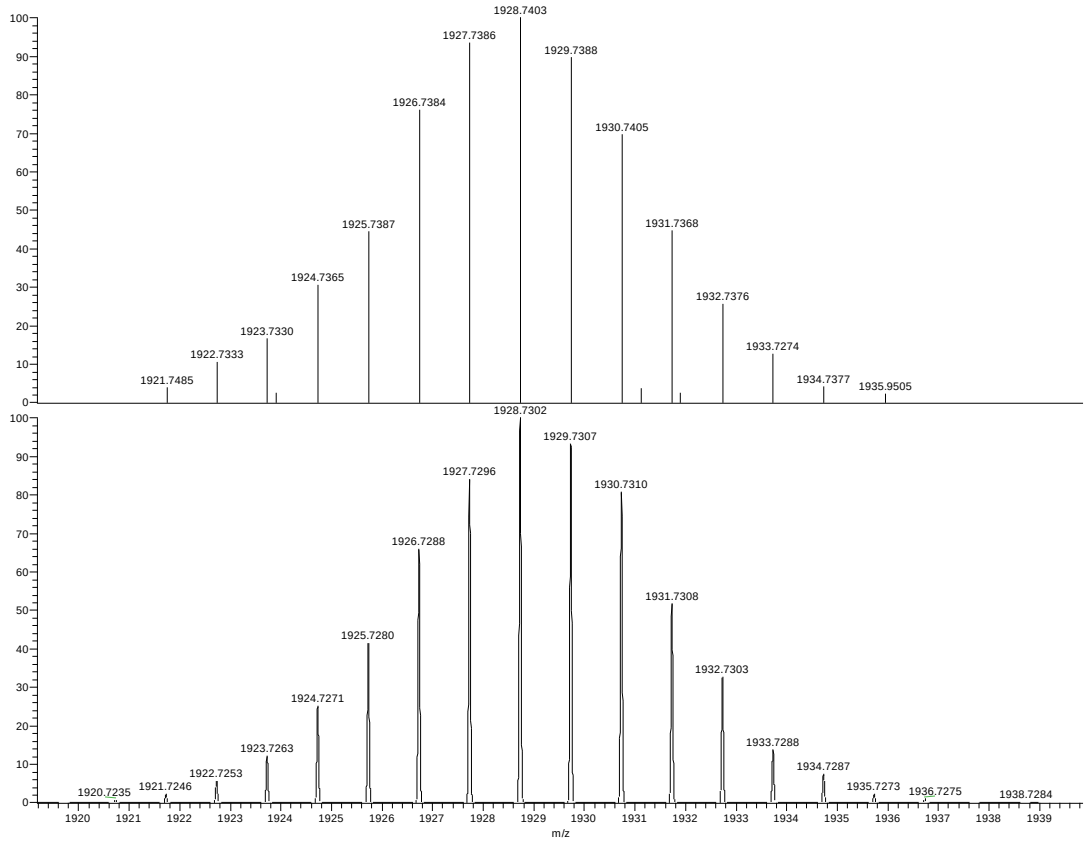

Figure S29. Measured (top) and simulated (bottom) spectrum of the fragment $[Ni_1Pb_6Bi_3]^-$.

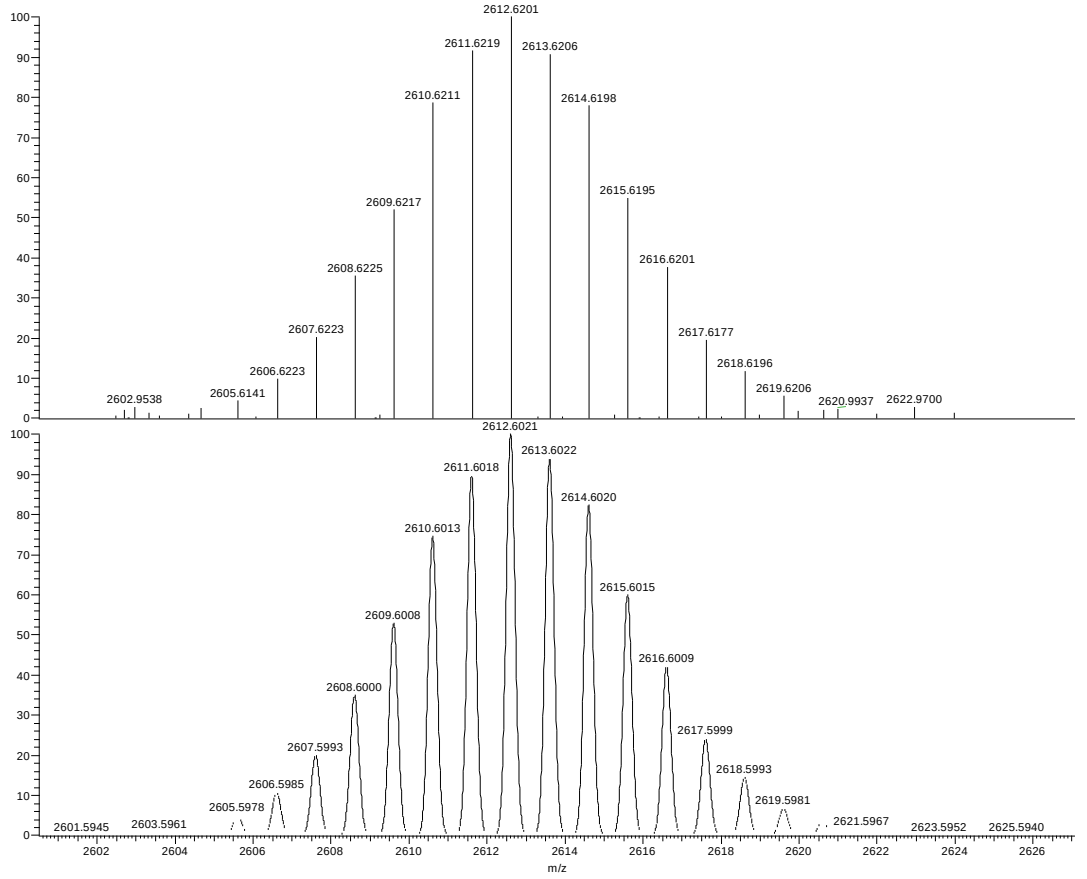

Figure S30. Measured (top) and simulated (bottom) spectrum of the fragment $[Ni_2Pb_7Bi_5]^-$.

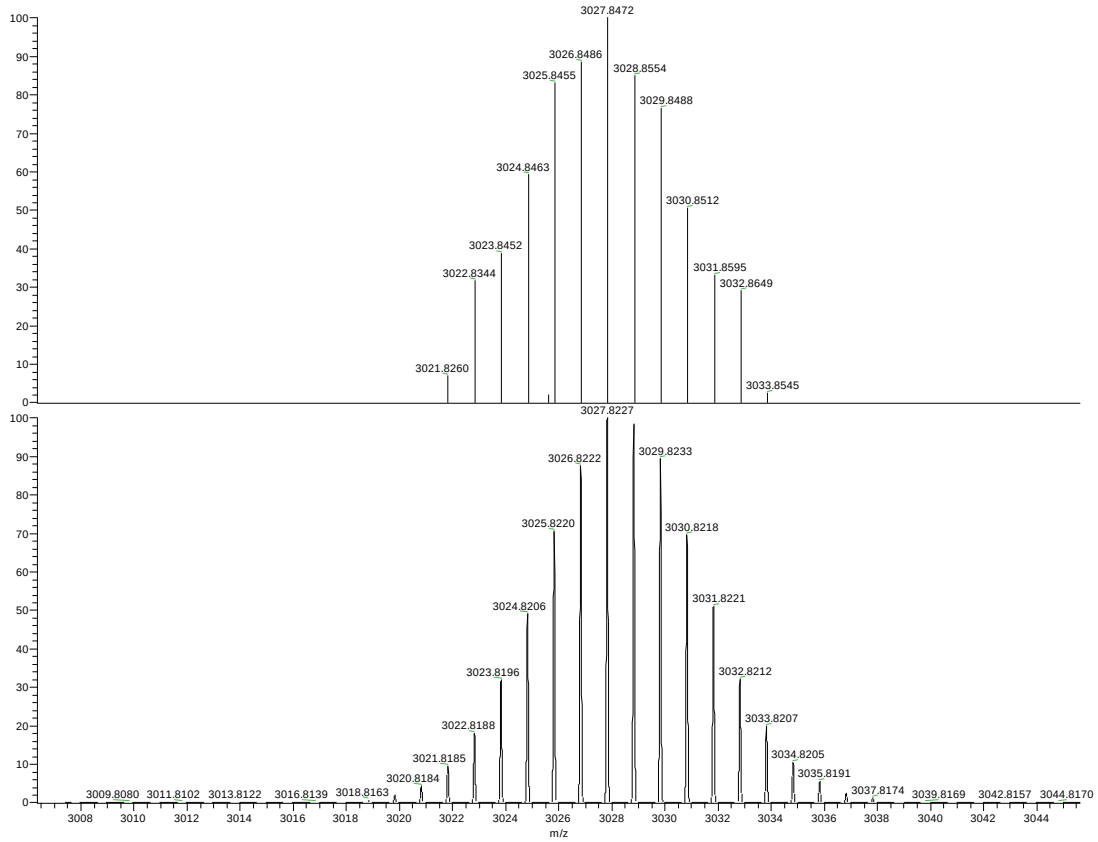

Figure S31. Measured (top) and simulated (bottom) spectrum of the fragment $[K_1crypt_1Ni_2Pb_7Bi_5]^-$.

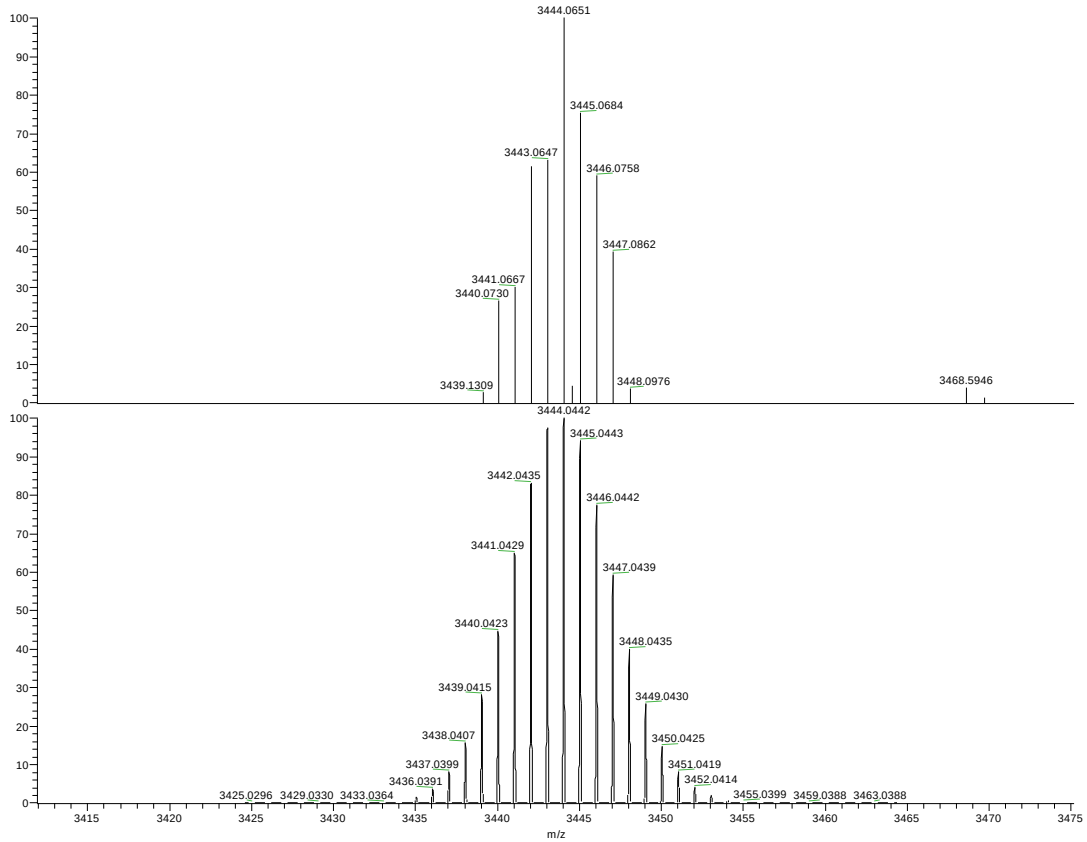

Figure S32. Measured (top) and simulated (bottom) spectrum of the fragment $[K_2crypt_2Ni_2Pb_7Bi_5]^-$.

Investigation of compound 4: At lower m/z = 1800-2300, molecular peaks characteristic to the Pb/Bi nine-atom cage were observed. However, in the higher m/z = 3000 – 3520 region, significant peaks occur that are characteristic to cluster **4** in the presence of [K([2.2.2]crypt)], showing a good stability and solubility under these conditions (Figure S33).

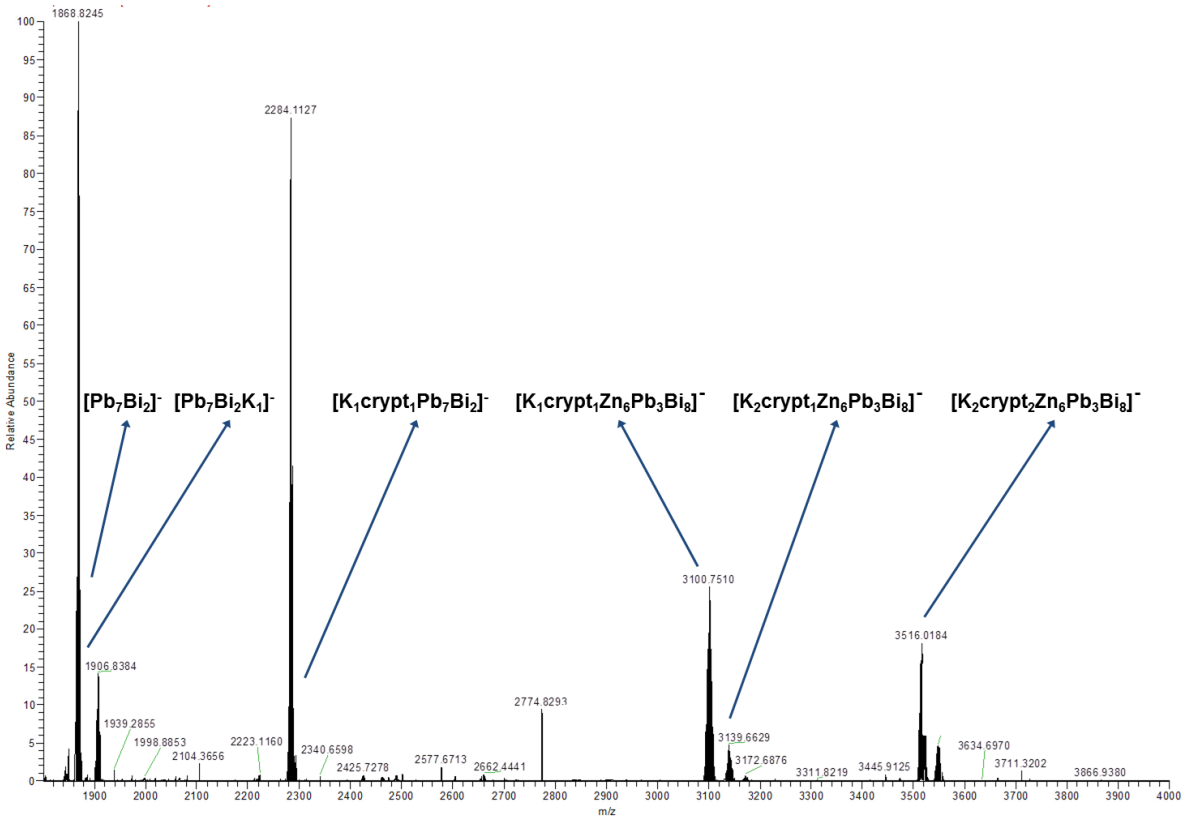

Figure S33. Overview ESI mass spectrum, recorded immediately upon injection of a fresh solution of hand-selected single crystals of **4** in DMF.

Figure S34 – Figure S39 show zooms of identifiable peaks of **4**:

at m/z = 1868.82; nine-atom fragment $[Pb_7Bi_2]^-$

at m/z = 1906.83; nine-atom fragment $K_1Pb_7Bi_2$

at m/z = 2248.11; nine-atom fragment $K_1crypt_1Pb_7Bi_2$

at m/z = 3100.75; fifteen-atom fragment $K_1crypt_1Zn_6Pb_3Bi_8$

at m/z = 3139.60; fifteen-atom fragment $K_2crypt_1Zn_6Pb_3Bi_8$

at m/z = 3515.77; fifteen-atom fragment $K_2crypt_2Zn_6Pb_3Bi_8$

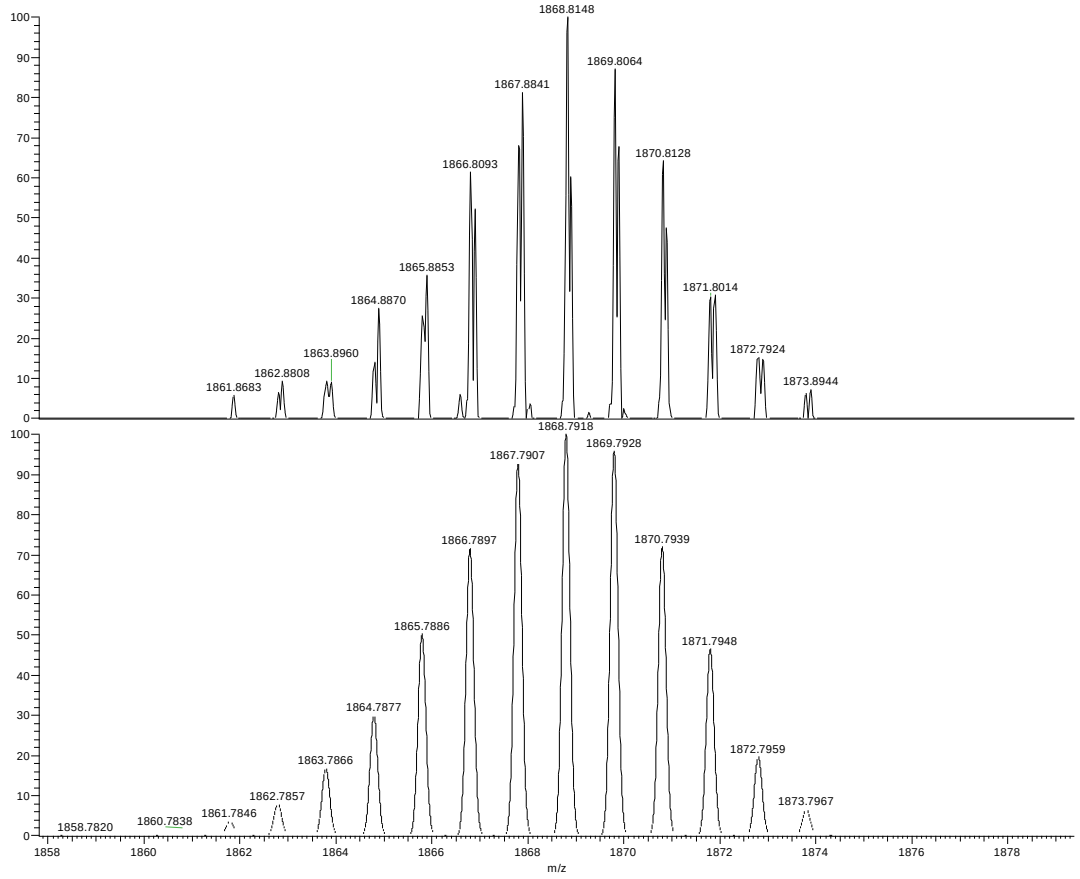

Figure S34. Measured (top) and simulated (bottom) spectrum of the fragment $[Pb_7Bi_2]^-$.

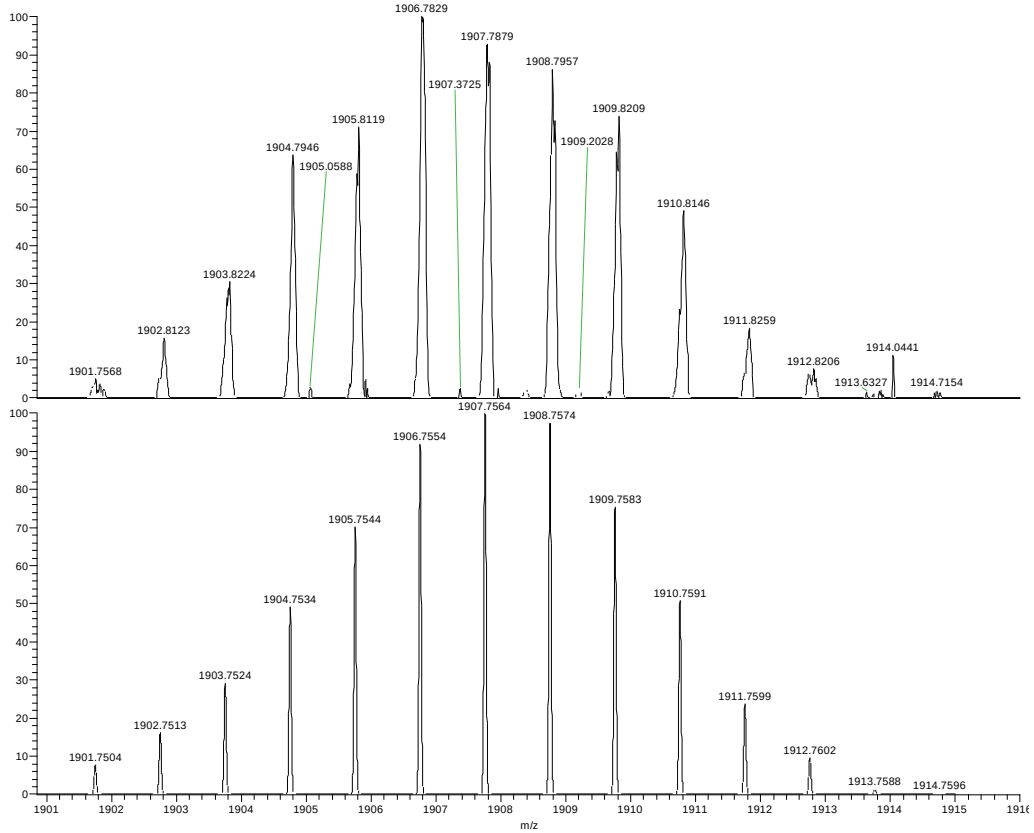

Figure S35. Measured (top) and simulated (bottom) spectrum of the fragment $[K_1Pb_7Bi_2]^-$

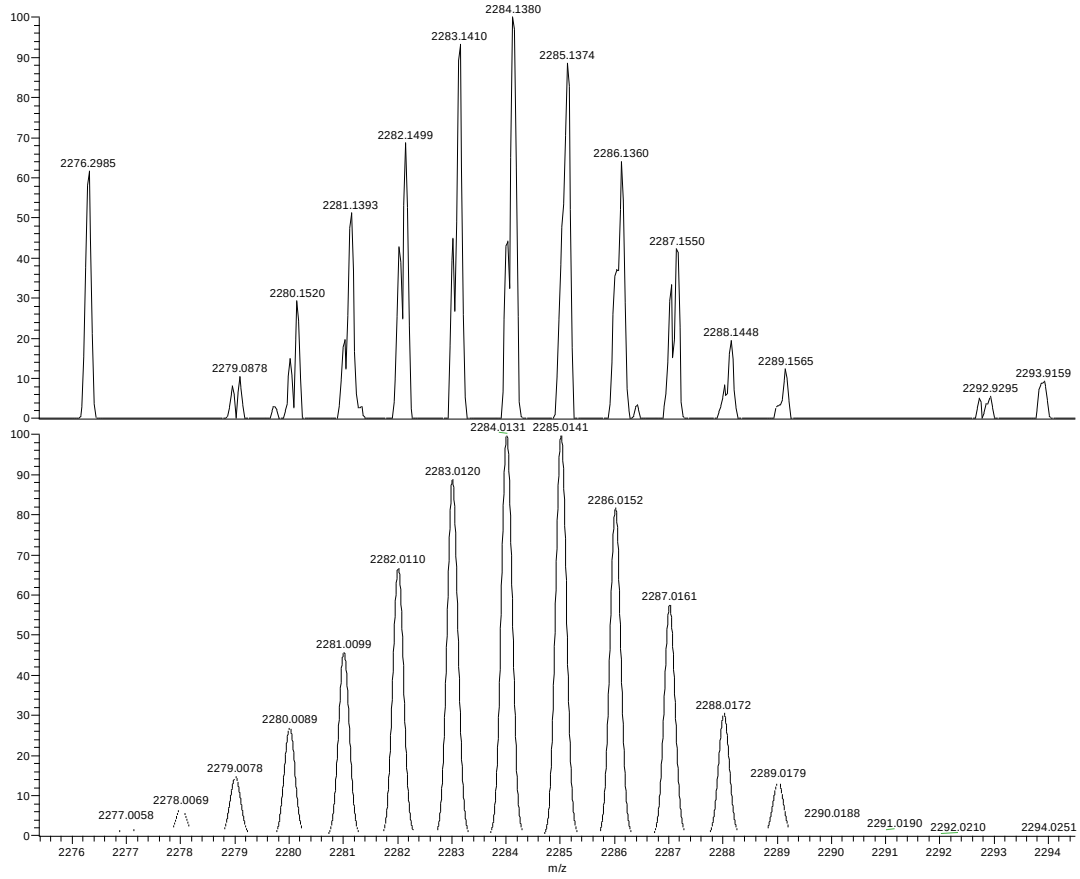

Figure S36. Measured (top) and simulated (bottom) spectrum of the fragment $[K_1crypt_1Pb_7Bi_2]^-$.

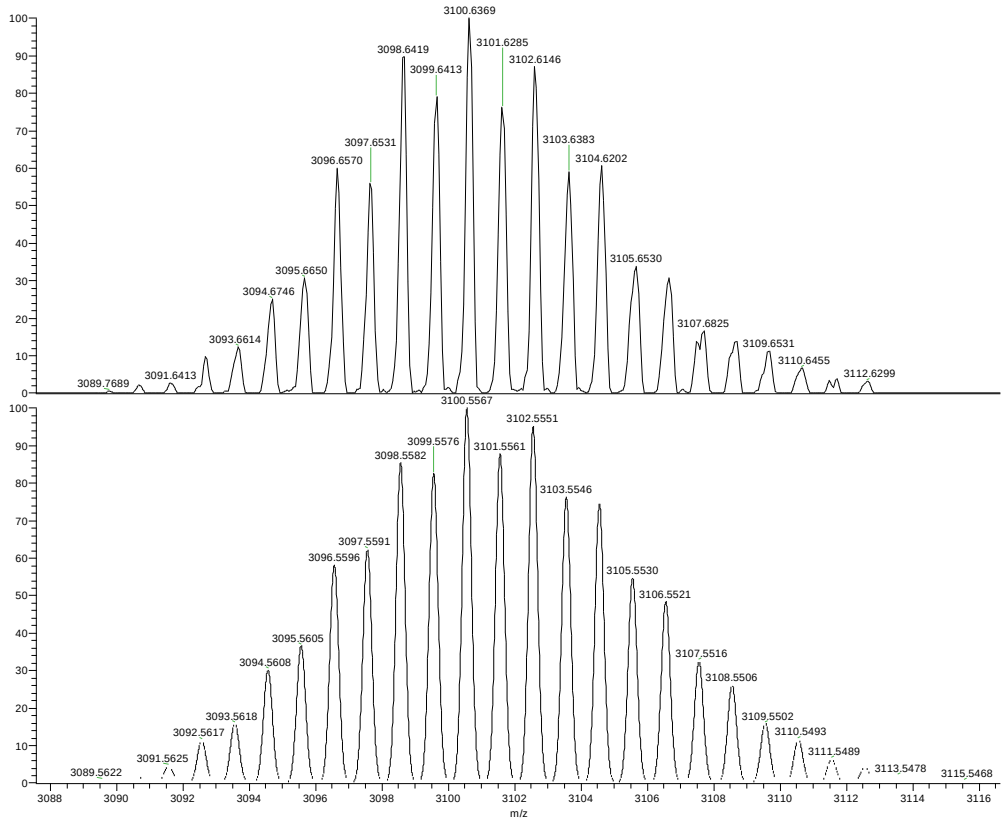

Figure S37. Measured (top) and simulated (bottom) spectrum of the fragment $[K_1crypt_1Zn_6Pb_3Bi_8]^-$.

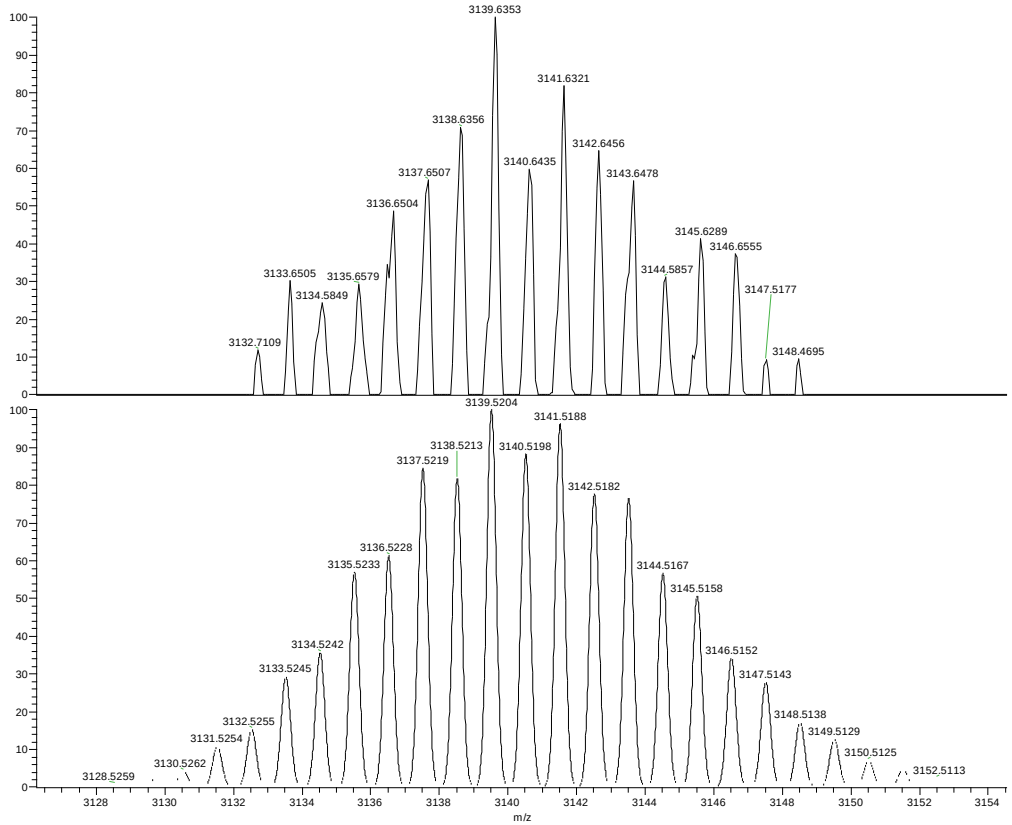

Figure S38. Measured (top) and simulated (bottom) spectrum of the fragment $[K_2crypt_1Zn_6Pb_3Bi_8]^-$.

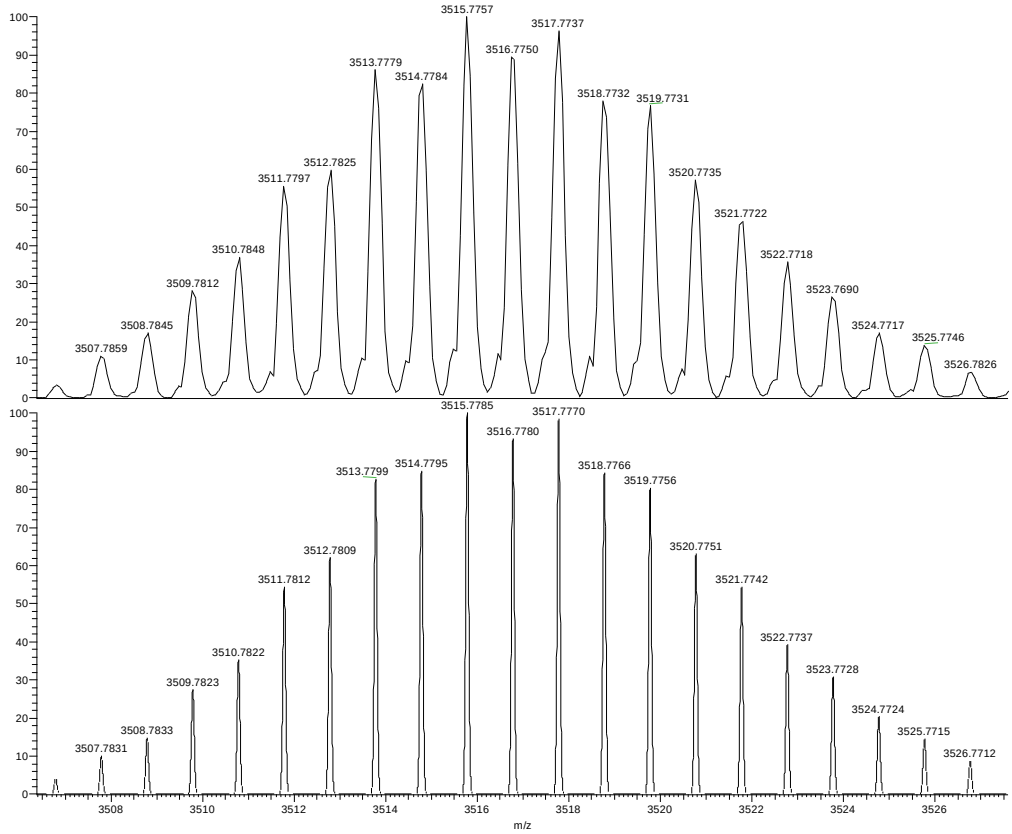

Figure S39. Measured (top) and simulated (bottom) spectrum of the fragment $[K_2crypt_2Zn_6Pb_3Bi_8]^-$.

5. Energy dispersive X-ray spectroscopy (EDX analyses)

EDX analyses were performed to check the elemental compositions of **1** - **4**; these could not be derived from the XRD experiments since Pb^{-} and Bi atoms are not distinguishable with certainty due to the very similar electron density. The EDX analyses were carried out using an EDX-device Voyager 4.0 of Noran Instruments coupled with an electron microscope CamScan CS 4DV. Data acquisition was performed with an acceleration voltage of 20 kV and 100 s accumulation time. The radiation emitted by the atoms was analyzed: Pb-L, Bi-L, K-K, Zn-K, Ni-K (Table S2). For the analyses, multiple single crystals or fragments from the as-prepared $K(Pb,Bi)_2$ phase were used and the data recorded both: various times on one single crystal/fragment and various times on other single crystals/fragments.

Table S2. EDX analysis of the as-prepared **$K(Pb,Bi)_2$** phase, **1**, **2**, **3** and **4** (Bi, Pb, K, Ni, Zn).

Element	k-ratio	ZAF	Atom %	Atomic ratio observed (calc)	Element wt %	wt % Err. (1-sigma)
$K(Pb,Bi)_2$ as prepared						
K-K	0.0528	1.588	32.77	1.8 +/- 0.0 (2)	8.39	+/- 0.13 (2%)
Pb-L	0.3979	1.041	30.56	1.7 +/- 0.2 (2)	41.44	+/- 3.86 (9%)
Bi-L	0.4835	1.038	36.68	2.0 +/- 0.1 (2)	50.17	+/- 2.38 (5%)
Total			100	5.5 (6)	100	
1						
K-K	0.0537	1.566	39.06	2.5 +/- 0.2 (2)	10.00	+/- 0.60 (6%)
Pb-L	0.2762	1.047	29.69	1.9 +/- 0.1 (2)	40.25	+/- 1.60 (4%)
Bi-L	0.5583	1.043	31.25	2.0 +/- 0.2 (2)	42.75	+/- 3.73 (8%)
Total			100	6.4 (6)	100	
2						
K-K	0.0542	1.219	22.58	2.8 +/- 0.3 (3)	5.32	+/- 0.60 (11%)
Pb-L	0.4739	1.349	19.35	2.4 +/- 0.1 (2)	57.22	+/- 1.60 (3%)
Bi-L	0.3762	1.033	58.06	7.2 +/- 0.7 (7)	37.46	+/- 3.73 (10%)
Total			100	12.4 (12)	100	
3						
K-K	0.0238	1.586	15.79	2.6 +/- 0.1 (3)	3.77	+/- 0.21 (6%)
Ni-K	0.0517	0.821	11.83	2.0 +/- 0.1 (2)	4.24	+/- 0.28 (7%)
Pb-L	0.4669	1.037	38.25	6.5 +/- 0.3 (7)	48.41	+/- 2.47 (5%)
Bi-L	0.4219	1.033	34.13	5.7 +/- 0.3 (5)	43.57	+/- 2.65 (6%)
Total			100	16.8 (17)	100	
4						
K-K	0.0477	1.555	20.64	4.1 +/- 0.5 (4)	7.42	+/- 0.83 (11%)
Zn-K	0.1575	0.826	28.82	6.0 +/- 0.8 (6)	13.01	+/- 1.82 (14%)
Pb-L	0.1974	1.088	14.85	3.1 +/- 0.7 (3)	21.47	+/- 4.70 (22%)
Bi-L	0.5360	1.084	36.09	7.5 +/- 0.7 (8)	58.10	+/- 5.62 (10%)
Total			100	20.7 (21)	100	

6. Powder X-ray diffraction

The as-prepared $K(Bi,Pb)_2$ phase was characterized via its X-ray powder diffraction pattern, measured on a Panalytical X'Pert Pro PW3040/60, equipped with Cu-Kα radiation under anaerobic conditions. Measurements under air failed in that the observed reflections could be assigned to the main group metal oxides. Figure S40 provides comparisons with the literature single crystals data of $K(Pb,Bi)_2$[5a] and KBi_2.[5b]

a)

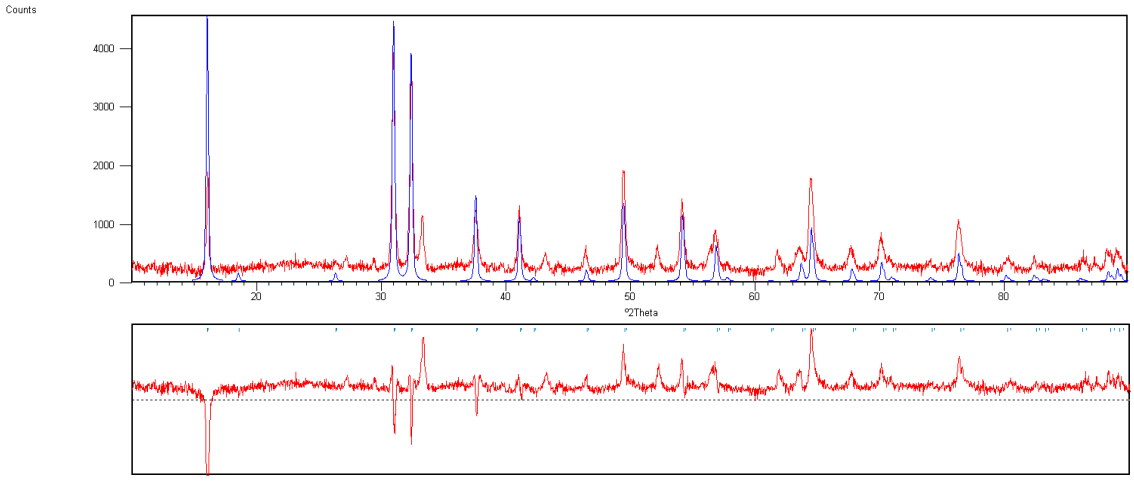

b)

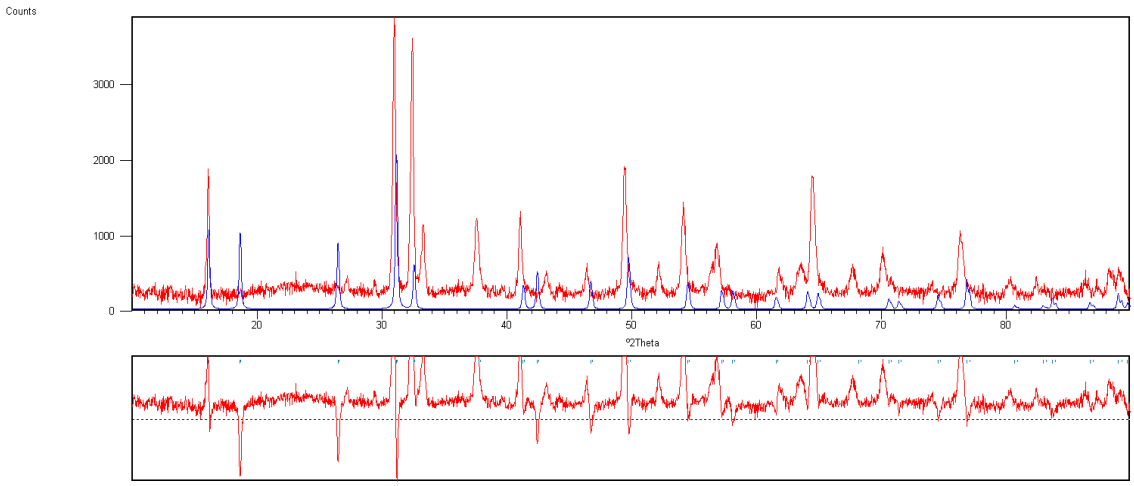

Figure S40. Comparison of the powder X-ray diffraction (PXRD) diagram of the as-prepared "KPbBi" phase (red lines) with PXRD simulations of single crystals data (blue lines) of $K(Pb,Bi)_2$[5a] (top) and KBi_2[5b] (bottom). The difference diagrams are given below each comparison.

The comparisons show a good fit with $K(Pb,Bi)_2$ from the literature, despite some differences in the intensities. They do not suggest the additional reflections at 33, 43, 52 and 62° in 2θ to derive from KBi_2. These might rather derive from traces of the known phase Pb_7Bi_3 (Figure S41).[5c]

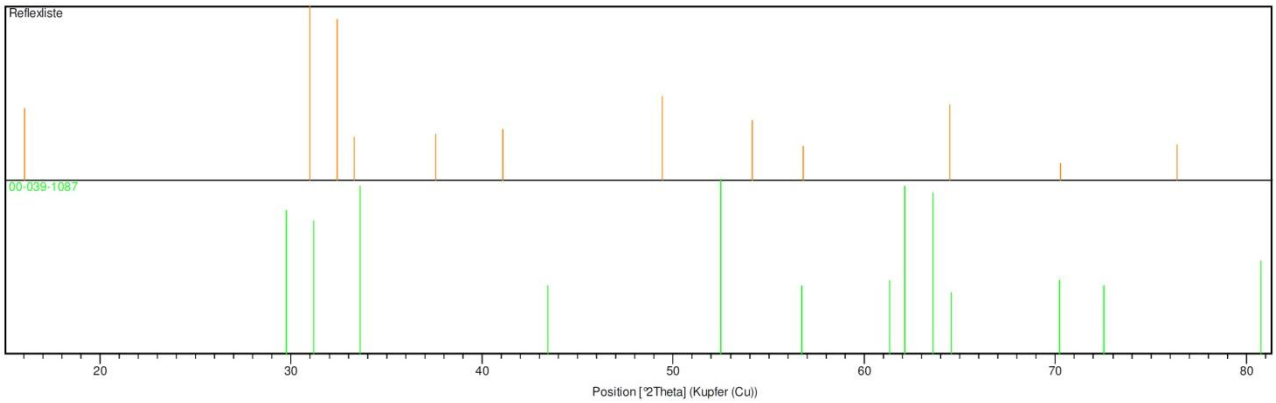

Figure S41. Comparison of powder X-ray diffraction data of the as-prepared “KPbBi” phase (top, orange) and those reported for Pb_7Bi_3 (bottom, green), indicating a clear mismatch.

6. Infrared spectroscopy

The FIR measurements of **3** and **4** (in transmission, Figures S42 and S43) were performed on a TENSOR 37 FT-IR spectrometer (Bruker). The samples were placed between two polyethylene pellets as a nujol suspension.

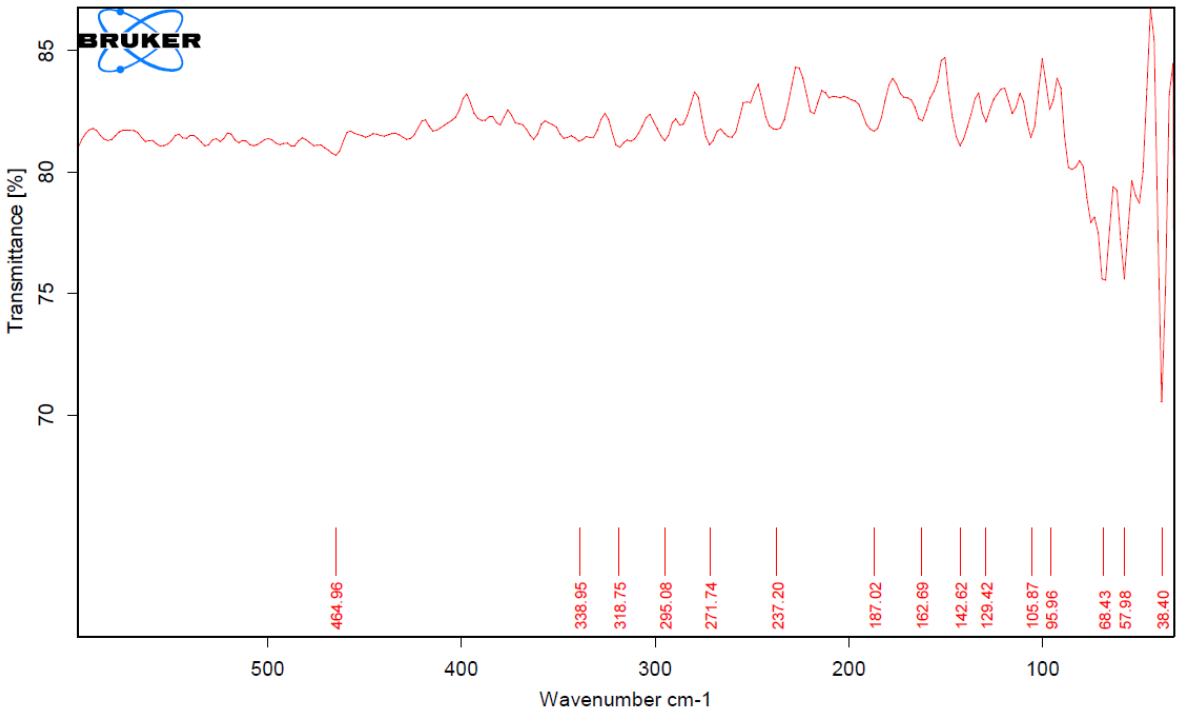

Figure S42. Infrared spectrum of single-crystalline **3**.

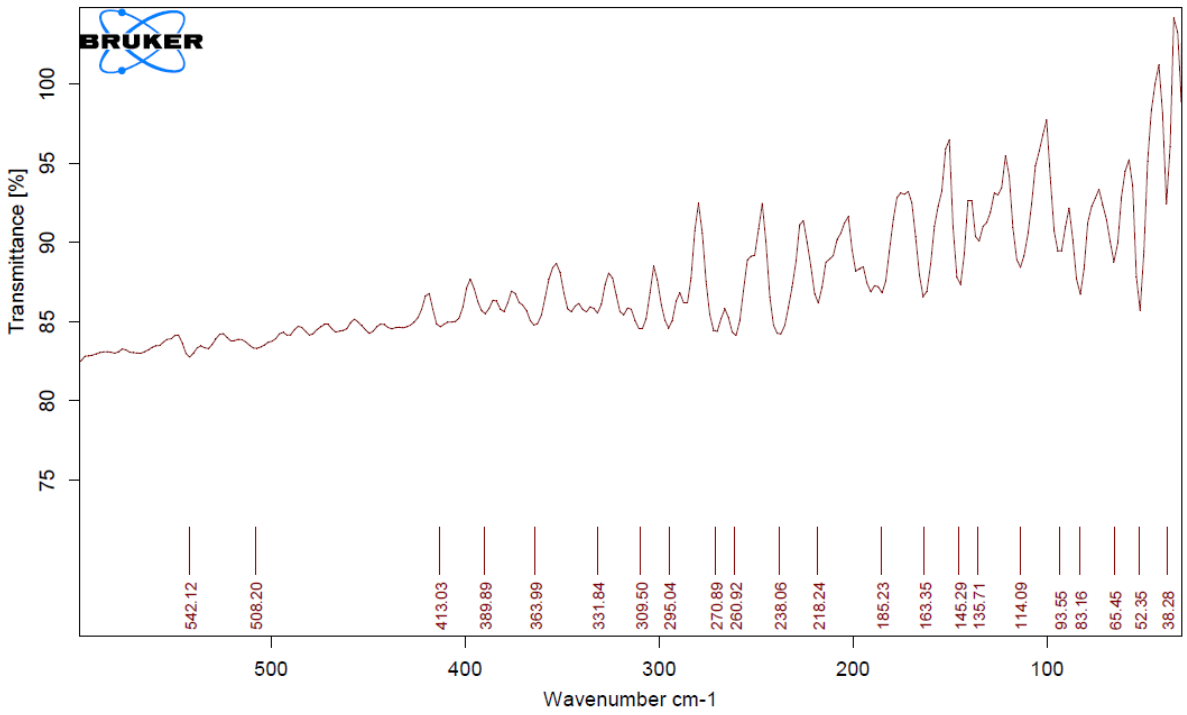

Figure S43. Infrared spectrum of single-crystalline **4**.

7. Methods of the quantum chemical investigations

DFT Calculations were done with the program system TURBOMOLE[6] employing the Becke–Perdew 86 (BP86) functional[7] with def2-TZVP bases[8] and respective fitting bases[9] for the evaluation of the Coulomb matrix. Effective core potentials (ECPs) were used for Sn (ECP-28), Pb (ECP-60) and Bi atoms (ECP-60).[10] Counter ions were modeled by the COSMO model with default parameters.[11] Figures S44 and S45 show the structures of the most stable isomers of the calculated species $[T_2Bi_2]^{2-}$, $[T_7Bi_2]^{2-}$, $[Ni_2T_7Bi_5]^{3-}$ and $[Zn_6T_3Bi_{11}]^{4-}$ (T = Pb, Sn) along with their total energies (1 a.u. = 1 Hartree = 2625.47 kJ·mol^{-1}) and dielectric contributions (dc), to be subtracted for consideration of the interaction of the anion with the model dielectric medium; energies of Pb or Sn atoms are −193.0064585173 a.u. (dc −0.0049350325 a.u.) or −214.3894882622 a.u. (dc −0.0032484925 a.u.), respectively for the same methods. Calculated distances are provided in Table S4.

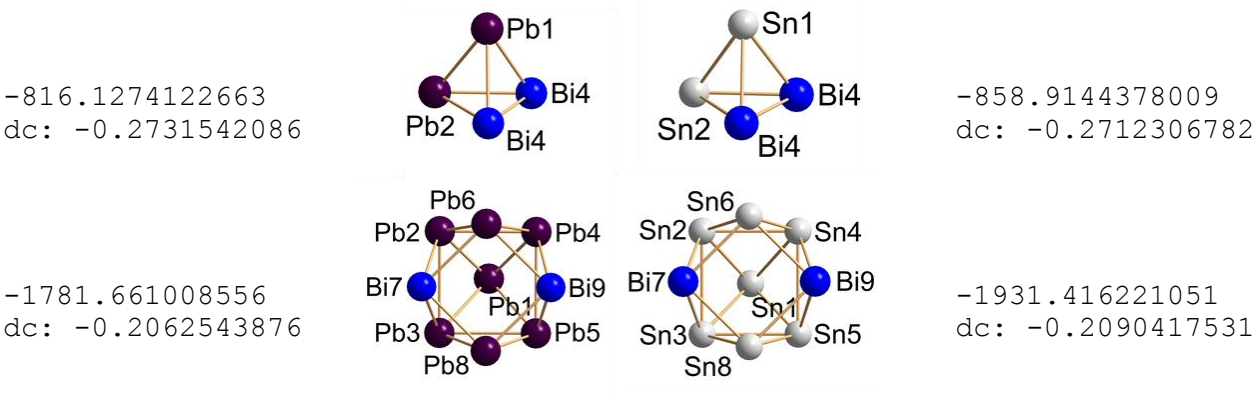

Figure S44. Molecular structure of the most stable isomers of $[T_2Bi_2]^{2-}$ and $[T_7Bi_2]^{2-}$ (T = Pb: left, T = Sn: right) along with their total energies and dielectric contributions (dc) [a.u.].

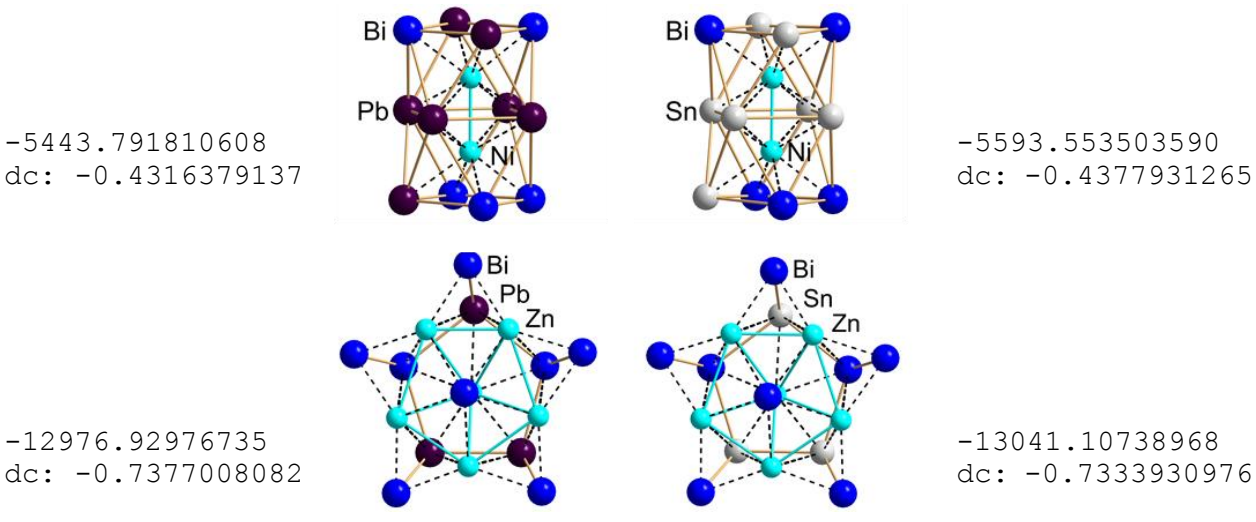

Figure S45. Molecular structure of the most stable isomers of $[Ni_2T_7Bi_5]^{3-}$ and $[Zn_6T_3Bi_{11}]^{4-}$ (T = Pb: left, T = Sn: right) along with their total energies and dielectric contributions (dc) [a.u.].

Table S4. Calculated distances in the anions shown in figures S35 and S36 [pm].

$[Pb_2Bi_2]^{2-}$	$[Sn_2Bi_2]^{2-}$	$[Pb_7Bi_2]^{2-}$	$[Sn_7Bi_2]^{2-}$
Bi3-Bi4 302.58	Sn1-Sn2 294.73	Pb1-Pb2 311.85	Sn1-Sn2 298.47
Pb2-Bi4 307.76	Sn2-Bi4 300.93	Pb1-Pb3 311.86	Sn1-Sn3 298.48
Pb1-Bi4 307.96	Sn1-Bi4 300.94	Pb8-Bi9 311.98	Sn1-Sn5 298.73
Pb1-Bi3 308.12	Sn1-Bi3 301.14	Pb6-Bi9 311.99	Sn1-Sn4 298.74
Pb2-Bi3 308.22	Sn2-Bi3 301.16	Bi7-Pb8 312.12	Sn2-Sn6 303.94
Pb1-Pb2 309.38	Bi3-Bi4 302.74	Pb6-Bi7 312.14	Sn3-Sn8 303.95
		Pb1-Pb5 312.35	Sn4-Sn6 304.22
		Pb1-Pb4 312.36	Sn5-Sn8 304.24
		Pb2-Bi9 313.89	Sn6-Bi9 305.18
		Pb3-Bi9 313.89	Sn8-Bi9 305.18
		Pb4-Bi7 313.92	Bi7-Sn8 305.24
		Pb5-Bi7 313.92	Sn6-Bi7 305.25
		Pb2-Pb6 318.84	Sn2-Bi9 305.71
		Pb3-Pb8 318.84	Sn3-Bi9 305.71
		Pb4-Pb6 319.34	Sn4-Bi7 305.80
		Pb5-Pb8 319.35	Sn5-Bi7 305.81
		Pb2-Pb4 331.47	Sn3-Sn5 315.91
		Pb3-Pb5 331.47	Sn2-Sn4 315.92
		Pb4-Pb5 349.28	Sn4-Sn5 337.98
		Pb2-Pb3 350.50	Sn2-Sn3 338.53
		Pb	
$[Ni_2Pb_7Bi_5]^{3-}$	$[Ni_2Sn_7Bi_5]^{3-}$	$[Zn_6Pb_3Bi_{11}]^{4-}$	$[Zn_6Sn_3Bi_{11}]^{4-}$
Ni-Ni 252.40	Ni-Ni 247.66	Zn-Zn 292.22-329.39	Zn-Zn 286.87-325.83
Ni-Pb 272.82-279.97	Ni-Sn 263.97-270.00	Zn-Pb 307.00-351.35	Zn-Sn 297.82-346.32
Ni-Bi 266.73-274.42	Ni-Bi 270.86-272.52	Zn-Bi 272.91-344.24	Zn-Bi 272.90-343.95
Pb-Pb 340.10-349.63	Sn-Sn 328.30-338.04	Pb-Pb 324.84	Sn-Sn 309.78
Bi-Bi 305.33-305.34	Bi-Bi 305.62-305.63	Bi-Bi 303.09-303.10	Bi-Bi 303.96-304.16
Pb-Bi 310.06-347.29	Sn-Bi 303.79-343.17	Pb-Bi 305.93-321.07	Sn-Bi 298.03-314.28

For further insight in the bonding situation, localized molecular orbitals[13] (LMOs, Table S5) and bond indices[14] (Table S6) were generated and analyzed. For illustration of the slight differences between Pb and Sn compounds, surface potentials were calculated for the Ni cluster in compound **3** as an example (Figure S46). The contour plot was generated with gOpenMol.[12]

Table S5. Localized molecular orbitals (LMOs) of $[Ni_2Pb_7Bi_5]^{3-}$ and $[Zn_6Pb_3Bi_{11}]^{4-}$ characterized by the diagonal element of the Fock matrix in LMO basis, diag(fock), and the dominant atom contributions from a Mulliken analysis.

$[Ni_2Pb_7Bi_5]^{3-}$				
Bi3-Pb-ring				
No.(diag(fock))	dominant contributions (from Mulliken analysis)			
141(-0.243)	6bi 0.949	8bi 0.908		
142(-0.243)	6bi 0.949	9bi 0.908		
148(-0.215)	8bi 1.202	11pb 0.617		
149(-0.215)	9bi 1.202	11pb 0.617		
Bi2-Pb2-ring				
150(-0.212)	4bi 1.170	7pb 0.640		
151(-0.212)	4bi 1.171	10pb 0.640		
153(-0.209)	12bi 1.174	10pb 0.638		
154(-0.209)	12bi 1.175	7pb 0.638		
Bi2Pb2-ring to Pb4-ring				
147(-0.216)	12bi 1.056	1pb 0.203	5pb 0.203	13ni 0.161
152(-0.212)	4bi 1.105	2pb 0.249	3pb 0.248	13ni 0.143
144(-0.223)	1pb 0.607	3pb 0.600	7pb 0.345	13ni 0.192
145(-0.223)	5pb 0.608	2pb 0.600	10pb 0.345	13ni 0.191
Bi3Pb-ring to Pb4-ring				
143(-0.226)	6bi 0.916	3pb 0.385	2pb 0.385	14ni 0.180
146(-0.222)	5pb 0.593	1pb 0.593	11pb 0.341	14ni 0.183
155(-0.201)	9bi 1.113	5pb 0.259	2pb 0.185	11pb 0.128
156(-0.201)	8bi 1.113	1pb 0.260	3pb 0.185	11pb 0.128
Ni(d)				
157(-0.187)	14ni 1.745			
158(-0.187)	14ni 1.745			
159(-0.186)	14ni 1.895			
160(-0.184)	13ni 1.732			
161(-0.183)	13ni 1.873			
162(-0.181)	14ni 1.853			
163(-0.180)	13ni 1.824			
164(-0.180)	13ni 1.824			
139(-0.323)	14ni 1.939			
140(-0.292)	13ni 1.930			
$[Zn_6Pb_3Bi_{11}]^{4-}$				
Outer Bi to Pb/Bi/Zn				
212(-0.219)	13bi 1.257	4zn 0.701		
213(-0.218)	13bi 1.270	3zn 0.680		
198(-0.233)	8bi 0.950	13bi 0.947		
215(-0.204)	14bi 1.177	7pb 0.672		
202(-0.225)	14bi 1.220	4zn 0.711		
203(-0.225)	14bi 1.215	5zn 0.714		
217(-0.198)	15bi 1.191	10pb 0.656		
210(-0.220)	15bi 1.230	2zn 0.723		
200(-0.228)	15bi 1.205	3zn 0.749		
216(-0.198)	16bi 1.192	11pb 0.658		
209(-0.221)	16bi 1.227	2zn 0.734		
201(-0.227)	16bi 1.213	1zn 0.743		
211(-0.220)	17bi 1.253	5zn 0.706		
214(-0.218)	17bi 1.277	1zn 0.671		
197(-0.233)	9bi 0.950	17bi 0.946		
Pb/Bi-Ring				
204(-0.225)	10pb 0.692	11pb 0.685	2zn 0.386	6zn 0.198
205(-0.224)	9bi 1.111	7pb 0.524	5zn 0.176	6zn 0.127
206(-0.223)	8bi 1.111	7pb 0.528	4zn 0.169	6zn 0.130
207(-0.223)	9bi 1.109	11pb 0.523	6zn 0.156	1zn 0.119
208(-0.222)	8bi 1.115	10pb 0.523	6zn 0.145	3zn 0.123
12Bi to Zn-Ring				
199(-0.232)	12bi 1.134	1zn 0.487	2zn 0.169	
195(-0.239)	12bi 1.090	4zn 0.410	5zn 0.387	
196(-0.234)	12bi 1.124	3zn 0.472	2zn 0.211	

Table S6. Bond indices of $[Ni_2Pb_7Bi_5]^{3-}$ and $[Zn_6Pb_3Bi_{11}]^{4-}$ and analogous Sn compounds.

$[Ni_2X_7Bi_5]^{3-}$	X=Pb	X=Sn		$[Zn_6X_3Bi_{11}]^{4-}$	X=Pb	X=Sn
Bi3-X-ring				Outer Bi to Bi/X		
Bi8-Bi6	0.89118	0.87858		Bi13-Bi8	0.94635	0.93213
Bi9-Bi6	0.89121	0.87861		Bi14-X7	0.89390	0.93769
X11-Bi9	0.80761	0.79500		Bi15-X10	0.84567	0.88289
X11-Bi8	0.80752	0.79496		Bi16-X11	0.84881	0.88499
Bi2-X2-ring				Bi17-Bi9	0.94650	0.93546
X7-Bi4	0.81317	0.80325		Outer Bi to Zn		
X10-Bi4	0.81334	0.80308		Bi13-Zn3	0.78206	0.79259
Bi12-X10	0.81571	0.79856		Bi13-Zn4	0.78675	0.79779
Bi12-X7	0.81575	0.79849		Bi14-Zn4	0.80229	0.79483
X4-ring (middle)				Bi14-Zn5	0.80075	0.79247
X3-X1	0.33690	0.30669		Bi15-Zn2	0.81886	0.82223
X3-X2	0.27304	0.25666		Bi15-Zn3	0.84427	0.82862
X5-X2	0.33691	0.30673		Bi16-Zn1	0.83816	0.82508
X5-X1	0.31486	0.27716		Bi16-Zn2	0.82365	0.82136
Bi3-X-ring to middle X4-ring				Bi17-Zn1	0.78062	0.79083
X11-X1	0.31350	0.31963		Bi17-Zn5	0.79322	0.80324
X11-X5	0.31360	0.31950		Bi-X-ring		
Bi6-X2	0.30401	0.30092		Bi8-X7	0.61389	0.64628
Bi6-X3	0.30406	0.30106		X10-Bi8	0.60334	0.62349
Bi8-X1	0.31533	0.30942		X11-X10	0.52544	0.57330
Bi8-X3	0.29441	0.28857		X11-Bi9	0.60282	0.62201
Bi9-X2	0.29438	0.28877		Bi9-X7	0.60514	0.64083
Bi9-X5	0.31527	0.30926		Bi12 to Zn-ring		
Bi2-X2-ring to middle X4-ring				Bi12-Zn1	0.58727	0.57301
X0-X2	0.31592	0.32039		Bi12-Zn2	0.44921	0.49413
X10-X5	0.30157	0.30143		Bi12-Zn3	0.57815	0.57073
Bi12-X1	0.34348	0.33023		Bi12-Zn4	0.54317	0.55095
Bi12-X5	0.34334	0.33015		Bi12-Zn5	0.52961	0.54934
Bi4-X2	0.33930	0.32297		Zn-ring		
Bi4-X3	0.33899	0.32266		Zn2-Zn1	0.17421	0.18727
X7-X1	0.30141	0.30125		Zn3-Zn2	0.20000	0.20035
X7-X3	0.31601	0.32069		Zn4-Zn3	0.13033	0.14346
Ni to neighbors				Zn5-Zn1	0.13782	0.14824
Ni13-X1	0.37370	0.38508		Zn5-Zn4	0.21537	0.22011
Ni13-X2	0.39330	0.40106		Zn-ring to Bi/X-ring		
Ni13-X3	0.39335	0.40105		Bi9-Zn1	0.21527	0.20332
Ni13-X5	0.37352	0.38513		X11-Zn1	0.18150	0.19946
Ni13-X7	0.33374	0.35314		X10-Zn2	0.35960	0.35020
Ni13-Bi4	0.41440	0.46681		X11-Zn2	0.35291	0.34441
Ni13-X10	0.33386	0.35303		X10-Zn3	0.18897	0.20433
Ni13-Bi12	0.41753	0.47653		Bi8-Zn3	0.21941	0.20750
Ni14-X1	0.37618	0.39659		X7-Zn4	0.21776	0.24054
Ni14-X2	0.39045	0.38340		Bi8-Zn4	0.25904	0.25109
Ni14-X3	0.39036	0.38340		X7-Zn5	0.22459	0.24150
Ni14-X5	0.37623	0.39660		Bi9-Zn5	0.26315	0.24895
Ni14-Bi8	0.41814	0.45424		Bi/X-ring to Zn6		
Ni14-Bi6	0.41386	0.42545		Bi9-Zn6	0.18470	0.18828
Ni14-Bi9	0.41814	0.45427		Bi8-Zn6	0.17258	0.17297
Ni14-X11	0.32584	0.35531				
Ni-Ni						
Ni14-Ni13	0.15809	0.25181				

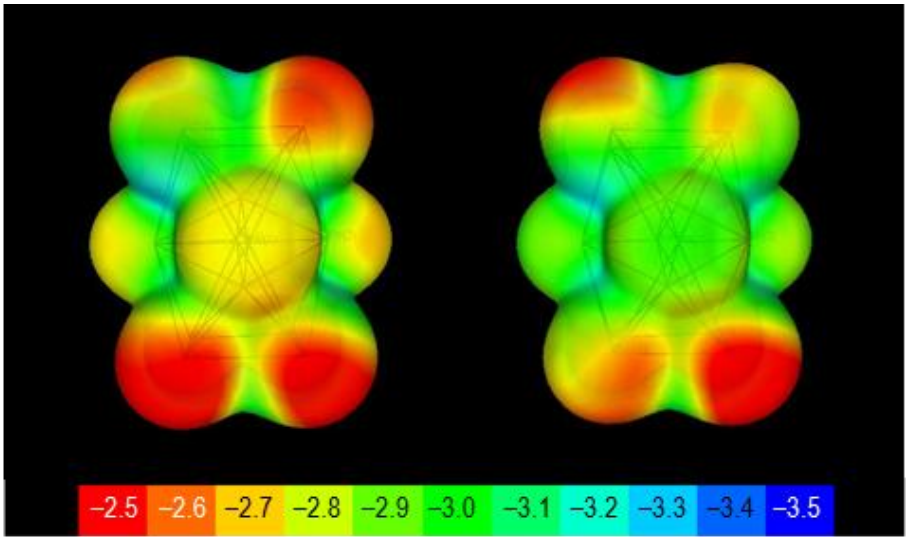

Figure S46. Illustration of electrostatic potentials *U* of the Ni/Pb/Bi anion in **3** (left) and its Ni/Sn/Bi analogue (right) from *U* = −0.25 a.u. (red) to *U* = −0.35 a.u. (blue), drawn as isodensity surfaces at 0.08 e·Å^{-3}. Warmer colors refer to lower surface potantials (−2.5 to −3.0, red to green), colder colors refer to higher surface potentials (−3.0 to −3.5, green to dark blue).

8. References for the supplementary information

1. (a) [2.2.2]crypt: 4,7,13,16,21,24-Hexaoxa-1,10-diazabicyclo[8.8.8]hexacosane; (b) S. Otsuka and M. Rossi, *J. Chem. Soc. (A)*, 1968, 2630.
2. E. N. Esentruk, J. Fettinger and B. Eichhorn, *J. Am. Chem. Soc.*, 2006, **128**, 9178.
3. (a) G.M. Sheldrick, SHELXL97, Program for the refinement of crystal structures, Universität Göttingen (1997). (b) DIAMOND Crystal and Molecular Structure Visualization, *Scientific Computing World*, 2002, **63**, 19. (c) H. D. Flack, *Acta Cryst.*, 1983, **A39**, 876. (d) A. L. Spek, *Acta Cryst.*, 1990, **A46**, c34.
4. S. C. Critchlow and J. D. Corbett, *Inorg. Chem.*, 1982, **21**, 3286.
5. (a) S. Ponou, N. Müller, T. F. Fässler and U. Häussermann, *Inorg. Chem.*, 2005, **44**, 7423; (b) F. Emmerling, N. Längin, D. Petri, M. Kroeker, C. Röhr, *Z. Anorg. Allg. Chem.* **2004**, *630*, 171; (c) S. E. Rasmussen and B. Lundtoft, *Powder Diffraction*, 1987, **2**, 28.
6. TURBOMOLE Version 6.2, (c) TURBOMOLE GmbH 2011. TURBOMOLE is a development of University of Karlsruhe and Forschungszentrum Karlsruhe 1989-2007, TURBOMOLE GmbH since 2007.
7. (a) A. D. Becke, *Phys. Rev. A*, 1988, **38,** 3098; (b) J. P. Perdew, *Phys. Rev. B*, 1996, **33**, 8822.
8. F. Weigend and R. Ahlrichs, *Phys. Chem. Chem. Phys.*, 2005, **7**, 3297.
9. F. Weigend, *Phys. Chem. Chem. Phys.*, 2006, **8,** 1057.

10. H. Stoll, B. Metz and M. Dolg, *J. Comput. Chem*., 2002, **23**, 767.
11. A. Klamt and G. Schürmann *J. Chem. Soc. Perkin Trans.*, 1993, **2**, 799.
12. D. L. Bergman, L. Laaksonen and A. Laaksonen, *J. Mol. Graph. Model.*, 1997, **15**, 301.
13. J. Pipek and G. Mezey, *J. Chem. Phys.*, 1990, **90**, 4916.
14. I. Mayer, *Chem. Phys. Lett*., 1988, **97**, 270.